Sanduni Ratnayake*, Johannes Lützenkirchen, Dieter Schild, Nicolas Finck, Elisabeth Eiche, Teba Gil-Díaz, Rohan Weerasooriya and Horst Geckeis

Solid phase speciation and mobility of thorium in soil samples from a case study in Sri Lanka

Abstract: Sri Lanka has high background radiation due to naturally occurring radionuclides like U-238, Th-232, and K-40 containing minerals. This study investigates the radiological characteristics of soil samples from the Matale District in central Sri Lanka, focusing on thorium (Th) and its potential mobility/bioavailability. Spectrometric data indi-cate that Th contributes most significantly to the elevated background radiation levels in this area. Thorium, present at approximately 0.2 wt.% in the bulk soil, was analyzed across various mineral phases, including oxides, silicates, and phos-phates, using multiple extraction and characterization tech-niques. Light rare earth elements (REEs) were also examined due to their natural association with Th-bearing minerals. This study provides, for the first time, relevant information on Th minerals in central Sri Lankan soil, addressing a critical research gap in radiological assessments of inland soils in the country. Findings provide insights into radiation exposure risks and the environmental behavior of radionuclides, serving as an important starting point for future studies on radioactive risk assessment in central Sri Lanka. The results contribute to the understanding of soil properties and emphasize the importance of further comprehensive studies to fully assess health risks and develop potential environmental safety measures.

Keywords: natural radionuclides; Th-minerals; light REE; selective extractions; environmental mobility; radioactive risk assessment

1 Introduction

The presence of minerals containing natural radionuclides (NRs) in soil is mainly inherited from the underlying geology and additionally influenced by the geographical setting. The mineral composition may have been modified over long periods due to weathering of the original rock material, with consequences for NR mobility in the environment.[1]

NR-containing minerals (monazite, thorianite, uraninite, etc.) occur in different amounts in various regions on earth.[1] In the relevant areas, U-238, Th-232, and K-40 constitute the major terrestrial components of natural background radiation, and together with their progenies, they significantly contribute to the total dose from natural sources. The mobility and chemical behavior of these radionuclides in geological settings play a major role in their distribution in the environment.[2]

Previous *in situ* natural radiation measurements by the Sri Lanka Atomic Energy Board (SLAEB) in comparison to observations in other regions in Asia suggest that Sri Lanka shows the highest average Th-232 concentration in soil. The mean value of Th radioactivity (including progenies) in Sri Lanka is 138 Bq kg^{-1} (ranging between 9 and 1,166 Bq kg^{-1}) [3] while the global average of natural Th-232 content in soil is 30 Bq kg^{-1} (ranging from 11 to 64 Bq kg^{-1}).[1] Areas with high background radiation levels (i.e., above worldwide average values) due to Th-rich monazite have been previously identified at Sri Lankan beaches where Th-containing minerals occur along with industrially valuable minerals including ilmenite, rutile, quartz, and zircon.[4–6] Among these minerals, some elements of economic interest (i.e., belonging to the technology critical elements) such as rare earth elements (REEs), are also associated with the monazite crystal structure, e.g., Lanthanum (La), Cerium (Ce), Neodymium (Nd).[7,8]

***Corresponding author: Sanduni Ratnayake**, Institute for Nuclear Waste Disposal, Karlsruhe Institute of Technology, Hermann-von-Helmholtz Platz 1, 76344 Eggenstein-Leopoldshafen, Germany, E-mail: sanduni.ratnayake@kit.edu. https://orcid.org/0000-0002-2857-2612
Johannes Lützenkirchen, Dieter Schild, Nicolas Finck and Horst Geckeis, Institute for Nuclear Waste Disposal, Karlsruhe Institute of Technology, Hermann-von-Helmholtz Platz 1, 76344 Eggenstein-Leopoldshafen, Germany. https://orcid.org/0000-0001-6034-8146 (D. Schild)
Elisabeth Eiche, Institute of Applied Geosciences, Karlsruhe Institute of Technology, Kaiserstraße 12, 76131 Karlruhe, Germany
Teba Gil-Díaz, Institute for Nuclear Waste Disposal, Karlsruhe Institute of Technology, Hermann-von-Helmholtz Platz 1, 76344 Eggenstein-Leopoldshafen, Germany; and Institute of Geosciences, Friedrich-Schiller-Universität Jena, Burgweg 11, 07749 Jena, Germany. https://orcid.org/0000-0003-2320-2708
Rohan Weerasooriya, National Institute of Fundamental Studies, Hantana Road, 20000 Kandy, Sri Lanka

The East Coast deposits in Pulmudei and Kokilai are the largest Th-bearing beach sand deposits in Sri Lanka.[9] Similar deposits were found in several coastal areas all over the island including the West Coast deposits in Kalutara, Induruwa, and Kaikawala.[10]

Yet, higher background radiation levels were discovered at a particular location in the inland of Sri Lanka called the Kawudupelella area (Matale district) while exploring the occurrence of natural radioactive minerals in 2015. SLAEB, in collaboration with the Geological Survey and Mining Bureau (GSMB) of Sri Lanka,[11] measured background radiation levels at a one-meter height above the ground of 21.6 ± 10.9 mSv yr^{-1} [12] notably exceeding the global average background radiation level of approximately 2.4 mSv yr^{-1}.[1] While the International Commission on Radiological Protection (ICRP) recommends a limit of 1 mSv yr^{-1} for public radiation exposure due to human activities (excluding medical and occupational exposure), this limit does not apply to natural background radiation.[13] Areas with high natural radiation exist globally without noted health risks; however, the elevated levels in this region, suggest the need for further evaluation of potential health risks associated with prolonged exposure. So far, a systematic study of measured activity levels in this area has not been available. The proximity of a public school and private buildings to the identified locations of increased radiation levels raises concerns related to potential health issues via direct exposure through external and/or internal pathways (radiotoxicity) for humans. Thorium near or at the soil surface is a health risk due to the generation of Ra-228 during the decay of Th-232, which emits gamma radiation [14] and gaseous Rn-220 (thoron) that may accumulate in closed rooms and contribute to the radiological exposure of lungs. Additionally, Th can enter the human body either when breathing in dust particles containing Th or when swallowing them with water or food, which may cause negative health effects.[15]

Besides the general knowledge concerning the site-specific soil properties, it is important to properly characterize the mineral content. In a second step, it is necessary to investigate the different chemical forms or association of trace element of interest in the soil. This information will help identifying potential solid carrier phases of trace elements of interest, and thus, predicting the behavior of NRs/stable elements and their potential bioavailability once they have been mobilized. The identification of such solid phases could help interpret or predict trace element transport related to direct rock weathering and/or trace element adsorption (i.e., after mineral dissolution or trace element solubilization).

In a previously published study, Sri Lankan soil samples from the Matale District presenting higher than average background radiation levels due to natural radioactive Th-232 had been thoroughly characterized.[16] The identified compounds included Th-phosphate (76 ± 2 %) and Th-oxide (24 ± 2 %) with minor amounts of thorite (silicate). Additionally, accessory minerals such as iron oxyhydroxides and clay minerals were detected, although a clear association of Th or Ln to such phases could not be established. Binding to accessory or secondary phases could, for example, be taken as an indication for potential mobilization of Th under given conditions. The sensitivity limits of direct spectroscopic methods at trace concentrations can, however, restrict speciation information on certain metal ions, highlighting the need for complementary methods, like sequential and single extraction procedures, to offer further insights into elemental mobility and bioavailability. Together, these approaches provide a comprehensive understanding of Th distribution and its environmental implications.

The mobility of a particular solute in soil or sediment systems under natural conditions has traditionally been estimated by extraction methods using specific reagents. In this context, both single and sequential extraction procedures have been widely applied primarily to characterize operationally defined host phases of given trace metals in soil. Metal ions or radionuclides can be analyzed by highly sensitive atomic spectrometric methods, such as ICP-MS or nuclear spectroscopy, in extract solutions, providing insight into trace component speciation that complement rather than replace the information from direct spectroscopic techniques. Even though major shortcomings are associated with sequential extractions concerning the potential redistribution of the trace elements among solid phases, loss of sample during intermediate washing steps, and the non-selectivity of certain reagents to specific phases, they are still frequently used for assessing availability and mobility of trace elements in soil matrices.[17–20] Despite the need for larger amounts of sample, single extraction methods have also been widely employed for faster analysis and because they may help circumvent some of the aforementioned shortcomings.[21–23]

The present work aims at the radiological characterization of Sri Lankan soil samples from the Matale District and at determining Th potential mobility/bioavailability. Several characterization techniques and selected extraction schemes previously used for Th were applied, along with complementary analysis of light REEs, which naturally occur with Th-bearing minerals in the region. This research addresses a significant knowledge gap for inland regions of Sri Lanka, where only a limited number of studies have been conducted. By identifying previously unrecognized radionuclide-bearing minerals, the study contributes to understanding the environmental behavior of NRs and the potential public health risks. Results furthermore provide general information on environmental behavior of radionuclides, which under certain

conditions might be as well of interest in the context of nuclear waste disposal safety studies in the sense of natural analogue investigations. While this work is an initial step, it highlights the need for systematic sampling and broader assessments to fully evaluate the local radiological conditions and health implications.

2 Materials and methods

2.1 Target area

The targeted location is the playground of a public school in a village in the Matale District, adjacent to a forest and school buildings. The site lies at the eastern part of a small valley, ~360 m above sea level. The groundwater table is about 3–4 m below the surface, with flow direction towards the SE. Annual rainfall in the area averages 1,500–2,000 mm, peaking during the second inter-monsoon in October and November.[24] These environmental factors, groundwater flow and rainfall, are relevant to the potential mobility/bioavailability of radionuclides in the soil, impacting their environmental behavior.

The Matale District is located in the center of Sri Lanka (Figure 1a). On the geological map of the entire Matale District in Figure 1b, the legend shows some of the major mineral formations related to the area of interest. The Matale District is underlain by Precambrian crystalline rocks including meta-sedimentary rocks such as marble, garnet-sillimanite-biotite gneiss quartzite and calc gneiss. The meta-igneous rocks in this area are represented by granitic orthogneiss and charnockite. Generally, these meta-sedimentary and meta-igneous rocks are intercalated with each other in the entire district.[25] Dharmapriya *et al.* (2020) investigated the geology in a location less than 5 km from our study site. According to that study, the main rock types that dominate in the vicinity of our study area are identified as marble, quartzite, khondalite, and garnet-sillimanite-biotite gneisses, garnetiferous quartzofeldspathic gneiss, biotite-hornblende gneiss and charnockite.[26] In Figure 1c, our area of interest is shown by a white cross. The major bed rock in this area seems to be an intercalation of some major rock formations, such as granite gneiss, biotite gneiss-and-granite, garnetiferous quartzofeldspathic gneiss, marble, and pegmatite (from left to right according to the map in Figure 1c). The intercalation of these rock formations contributes to high radiation levels due to their NRs content, including U-238, Th-232 and their decay products as well as K-40.[27–30]

The playground soil is primarily lateritic, rich in kaolinite and Fe/Al oxides, formed under hot and humid climate with subsequent alternating wet and dry periods.[31] These soils are acidic,[31] with pH below 5.5,[32] which favors the mobility of harmful cations and enhances plant uptake, potentially leading to their accumulation in the food chain and related health risks.[15,32,33]

2.2 Sampling and pretreatment

Sampling locations were selected after measuring background radiation levels at one-meter height above the ground using a radiation survey meter equipped with a NaI scintillation detector and a built-in GM counter (model: Automess 6150 AD5/H).

In total, four soil samples, L-03 (07° 34.687′, 80° 37.695′), L-04 (07° 34.691′, 80° 37.695′), L-05 (07° 34.699′, 80° 37.689′), and L-06 (07° 34.707′, 80° 37.683′), were collected on July 15th 2017 at the school playground of Kawdupalella, Matale District, Sri Lanka (Figure 2). These samples were collected following the IAEA judgmental sampling approach.[34] A mass of about 1 kg of soil per sample was obtained by removing the top layer (to minimize anthropogenic contamination) and then scooped up from a depth of 10–20 cm below the surface with a shovel. All samples were packed in polyethylene bags and transported to the SLAEB laboratory in Colombo, Sri Lanka, where non-target materials, such as plant debris and large stones, were manually removed. After air-drying for 24 h, the soil samples were sieved through 2 mm mesh-sized sieves. All samples were packed in plastic containers and shipped to Germany in November 2017 (all the respective regulations were followed including the disposal of the material after the experimental work).

2.3 Chemicals and solutions used for batch extractions

All chemicals were purchased from Merck (Germany), Alfa Aesar (Germany), VWR chemicals (USA and Belgium), Carl Roth (Germany), or Honeywell (USA) and were of analytical reagent grade. Dilutions and solution preparations were carried out using Milli-Q water (Milli-Q system, Millipore, 18.2 MΩ cm and maximum total organic carbon 2 µg L^{-1}).

2.4 Characterization of soil samples

2.4.1 Gamma spectrometric analyses

Activity concentrations of radionuclides in the soil samples were determined by gamma spectrometry at SLAEB involving a high-purity germanium detector, HPGe (Canberra, model: Gx3020), with a relative efficiency of 32.6 %. A

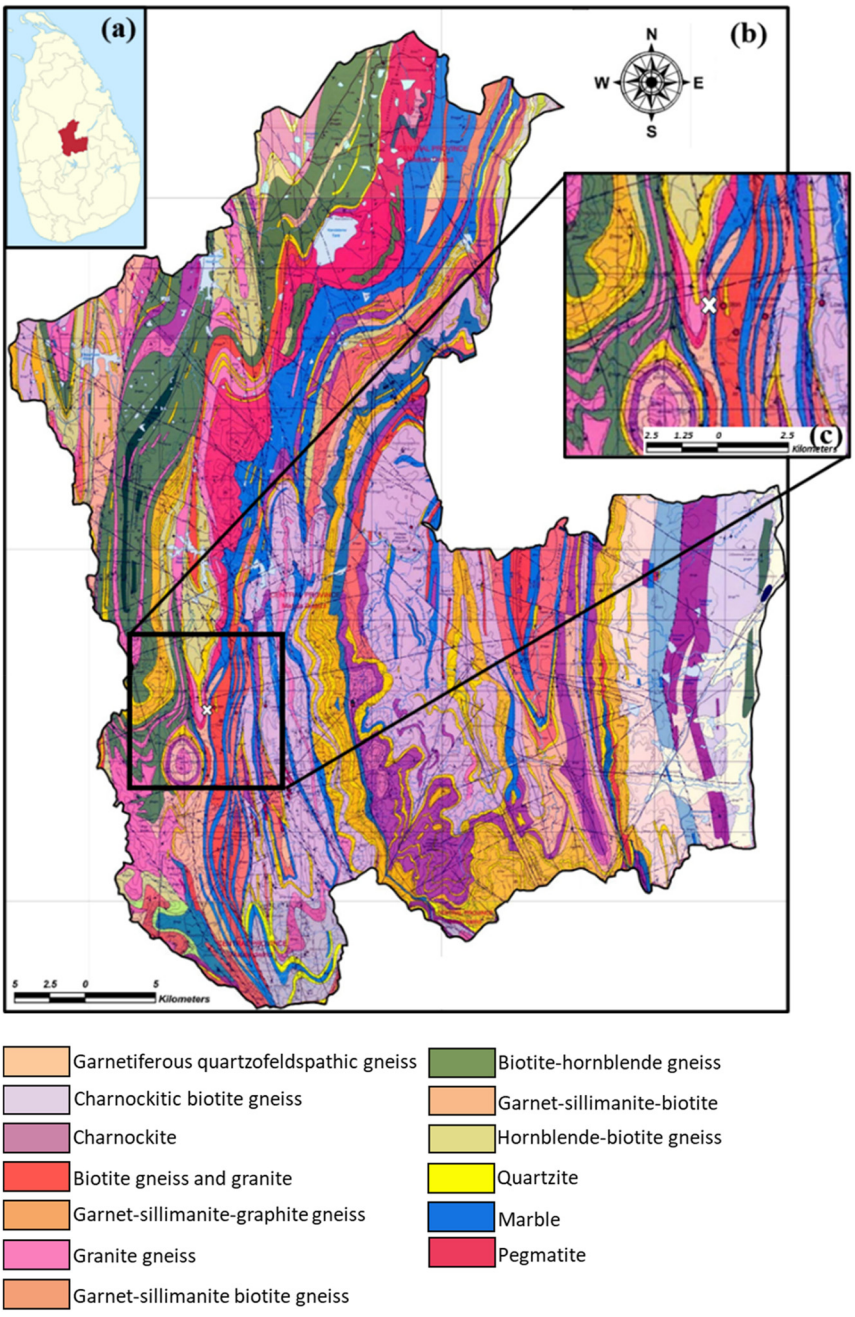

Figure 1: Geological map of the Matale District. (a) Matale District shown in the map of Sri Lanka, (b) detailed geological map of the Matale District (provided by the Geological Survey and Mines Bureau, Sri Lanka on request), and (c) magnified map reference to the target area of the present study (the location of the study area where samples were collected is shown by a white cross).

mass of 100 g of each soil sample was kept in well-sealed plastic vials separately to prevent the escape of radiogenic gases (Rn-222 and Rn-220 generated from U-238 and Th-232 decay series, respectively). Those samples were sealed for one month to attain secular equilibrium with the respective mother nuclides Ra-226 and Ra-224, and then subjected to gamma spectrometric analysis.

Calibration of the detector involved both energy and efficiency calibration. Energy calibration was done using a point source containing Cs-137 (661.5 keV) and Co-60 (1,173.2 and 1,332.5 keV). For efficiency calibration, IAEA-certified reference material, a standard soil of known radioactivity – Soil 6, was used to validate the accuracy of the measurement across a wide range of gamma energies, including 1,460 keV for K-40 and 2,614.5 keV for Tl-208 (a progeny of Th-232). To ensure the validity of the measurements, the soil samples and the reference material (IAEA Soil 6) were carefully matched in terms of composition and geometry. Both were prepared in the same type of containers, with identical masses and shapes, to maintain consistent counting geometry and reduce efficiency errors. Also, the validation process ensured that the energy and efficiency calibrations were appropriate for all

Figure 2: The school playground of Kawdupalella, Matale District, Sri Lanka. (a) Satellite view (from Google Earth with the imagery date of 1.3.2018); (b) magnified view of the location of interest (red area of (a)). Identifies for the sampling sites of the soil samples are "L", and the school buildings are denoted by "S".

radionuclides of interest, including those with high-energy gamma emissions. The use of Soil 6 as reference material ensured proper calibration for all radionuclides of interest. Detection limits for K-40, Ra-226, and Th-232 were determined to be 16.6 Bq kg^{-1}, 6.7 Bq kg^{-1}, and 7.6 Bq kg^{-1}, respectively, derived from the minimum detectable activity (MDA) for each isotope, using GENIE 2000 labsoc software.

Spectra were analyzed using GENIE 2000 data acquisition Canberra software. A counting time of 72,000 s for each sample was fixed to ensure statistical accuracy. The specific

activities of K-40, Ra-226, Th-232, and Pb-210 were obtained. For the estimation of U-238 activity (assuming secular equilibrium between U-238, Ra-226, and their progenies), energy peaks of 186.1 keV from Ra-226, 609.4, and 1,764.5 keV from Bi-214 were used, while for K-40 estimation, the photopeak energy of 1.46 MeV emitted by potassium itself was used. For Th-232 activity estimation, peaks of 911 keV from Ac-228, 238.6 keV from Pb-212, 583.1, and 2,614.5 keV from Tl-208 were used.[35] Note that Th-232 analysis requires being in secular equilibrium, whereas for its first daughter nuclide, Ra-228 with a half-life of 5.7 years, this is not necessarily the case. The derivation of Th-232 activity from Ac-228 activity and following progenies will be correct for refractory minerals but needs to be considered with care for samples having experienced significant chemical alteration. Details about the energy peaks of the progeny's gamma emission used to analyze the gamma data are shown in the Appendices (Table A1).

From the background corrected spectra of the samples the activities of radium, thorium and potassium were estimated using the following expression [35]:

$$A = \frac{N \times 100 \times 100}{\eta \times p \times W} \tag{1}$$

Where A represents the specific activity of a given radionuclide (in Bq kg^{-1}), N is the net count rate under the photopeak for a given gamma line under study, η is the photopeak efficiency of the detector system, p is the percentage gamma abundance of a particular gamma line, and W is the mass of the sample (in kg).

Uncertainties in the calculated activities were estimated by considering statistical counting uncertainties (Poisson statistics) and uncertainties in detector efficiency calibration. The total uncertainty (ΔA) for the activity concentration was derived using:

$$\Delta A = A \times \sqrt{\left(\frac{\Delta N}{N}\right)^2 + \left(\frac{\Delta \eta}{\eta}\right)^2} \tag{2}$$

Where ΔN and $\Delta \eta$ represent the uncertainties in the net count rate and detector efficiency, respectively.

2.4.2 Evaluation of radioactivity data

Air-absorbed dose rates were estimated by using the radionuclide activity concentrations of K-40, Ra-226, and Th-232 in the studied soil samples. These values were calculated according to Eq. (3) and Eq. (4).[1,36]

The absorbed dose rate in the air at 1 m height above the ground (D) due to gamma emissions from the U–Th series and K-40 was calculated using the measured gamma spectrometric results from the following equation.

$$D\left(nGy\,h^{-1}\right) = 0.0414\,C_K + 0.4611\,C_{Ra} + 0.623\,C_{Th} \tag{3}$$

Eq. (3) involves the dose coefficients in nGy h^{-1} per Bq kg^{-1}, while C_K, C_{Ra}, and C_{Th} are the measured activity concentrations of K-40, Ra-226, and Th-232 in Bq kg^{-1}, respectively.

The annual effective dose equivalent from external exposure to gamma rays from the soil samples (H_E) was estimated from the absorbed dose rate based on the following equation.

$$H_E\left(mSv\,yr^{-1}\right) = D\left(nGy\,h^{-1}\right) \times 8,760\left(h\,yr^{-1}\right) \times 0.2 \times 0.7\left(Sv\,Gy^{-1}\right) \times 10^{-6} \tag{4}$$

In Eq. 4, 0.2 is the outdoor occupancy factor and 0.7 Sv Gy^{-1} is the conversion factor for external gamma irradiation. The results were then compared with *in situ* gamma measurements (see Section 3.1).

2.4.3 pH measurements

The specific pH of the soil samples (supernatant after settling) was measured after mixing 10 g of soil sample with 50 mL of Milli-Q water. The samples were shaken repeatedly for 30 min and allowed to stand for 1 h [37] under an ambient atmosphere. A pH meter (Orion 720A+, Thermo Electron Corporation) and a pH electrode (Orion 8102BN, ThermoFisher Scientific) were used for this purpose and also later for pH adjustments of extractant solutions. The pH measurement set-up was calibrated before use with at least three buffers of known pH.

2.4.4 BET surface area

BET surface area measurements were carried out to determine the specific surface areas of the soil samples. The analyses were conducted using an AS1 (Autosorb1, Quantachrome), with nitrogen as the adsorbate at liquid nitrogen temperature (77 K). Prior to the measurement, the samples were degassed at 80 °C for 16 h to remove any adsorbed gases or moisture. The surface area values were calculated based on the nitrogen adsorption isotherms, involving the multi-point BET method. This information is relevant for understanding the adsorption and surface properties of the soil samples, especially in relation to retention and mobility of radionuclides.

2.4.5 Total organic carbon (TOC)

TOC values of the soil samples were estimated following the Walkey-Black wet oxidation method.[38] Briefly, volumes of 10 mL of 1 N $K_2Cr_2O_7$ and 20 mL of concentrated H_2SO_4 solution were added to 1 g of ground soil sample and left standing for 30 min. After adding about 200 mL of Milli-Q water and 10 mL of concentrated H_3PO_4, the mixture was

titrated with 0.5 mol L^{-1} ferrous ammonium sulfate solution in the presence of diphenylamine indicator until the color changed from violet-blue to green.

2.4.6 XRD analyses

X-ray diffraction patterns were recorded to gain information about the major mineralogical components of the bulk soil samples. An adequate mass (usually a few milligrams) of each sample was separately suspended in iso-propanol. Aliquots of the resulting suspensions were applied onto a low background silicon wafer using a pipette. In addition, the clay phases of all four bulk soil samples were separated by preparing a suspension in iso-propanol, sonicating, and decanting the suspension after a sedimentation period of about 1 min. The clay fraction remains suspended in the decanted fraction while the coarse material stays in the sedimented fraction. These clay samples were separately placed onto silicon wafers. Then all the samples were allowed to dry in a fume hood and subjected to XRD analysis using a D8 Advance X-ray diffractometer (Bruker AXS) at 40 kV and 40 mA operated using Cu-Kα radiation at λ = 0.15406 nm. The diffractograms were recorded by an energy dispersive detector (Sol-X) over the 2θ range of 2–80° using a step size of 0.015° and a counting time of at least 6 s per step. The evaluation was done by the Bruker AXS Diffrac^{Plus} EVA software (Bruker AXS, Germany, version 3.1). Phase identification was achieved by comparison with the PDF-2 database.

2.4.7 ATR-FTIR analyses

Fourier-transform infrared (FTIR) spectra were recorded to identify the main IR-active groups in the soil matrices using a Bruker IFS 55 spectrometer equipped with an attenuated total reflectance (ATR) accessory (MIRacle ATR single reflection diamond cell, PIKE Technologies, Madison, USA) and a DTGS (deuterated triglycine sulfate) detector. The soil samples were mildly ground with an agate mortar and pestle to obtain a homogeneous distribution without destroying the mineral phases. Those samples were mounted on the ATR sample stage and spectra were collected at 4 cm^{-1} resolution in the 400-4,000 cm^{-1} spectral range. The OPUS 7.5 software was used for data treatment.

2.4.8 X-ray fluorescence analyses

The elemental composition of the samples was determined by XRF spectroscopy. Samples were powdered using a vibratory agate disc mill before the analysis. Wavelength Dispersive XRF (WD-XRF, model: S4 Explorer, Bruker AXS) quantified the major components in the samples (i.e., SiO_2, Al_2O_3, Fe_2O_3, etc.). For the WD-XRF analysis, the powdered samples were heated to 950 °C to remove moisture and carbon/sulfur (i.e., sulfides and less stable sulfates)-containing compounds. The loss on ignition (LOI) was determined and the values were subsequently used to correct the data from WD-XRF. The ignited samples were mixed with Lithium tetraborate/Lithium metaborate (Spectroflux 110) and fused beads were produced using a fusion instrument with a final temperature of ~1,100 °C. A Rh X-ray tube (50 keV, 1 kW) was used as radiation source. The signals were detected using a proportional flow counter (Ar-CH_4 gas) and a scintillation counter. XS-55, LIF2000 und PET were taken as analyzer crystals. Energy-dispersive XRF (ED-XRF, model: Epsilon 5, PANalytical) was used for the detection of minor and trace elements (i.e., Th, La, Ce, and Nd) directly from the powdered samples. The bulk powder was filled into spectro cups that were sealed with a Mylar film of six mm thickness. A tungsten X-ray tube (80 kV, 600 W, 6 mA) was used as radiation source, whereas a Ge-detector was used for detection and quantification. In order to optimize the fluorescence measurements (improvement of signal-to-noise ratio), each sample was analyzed by consecutively using BRAKLA – polarization targets (Al_2O_3) and secondary targets (CaF_2, Fe, Ge, KBr, Zr, Mo, Ag, CsI). For calibration of both instruments, different certified rock and soil samples were used. Three certified standards, SY-2, SY-3, BE-N, were used for quality assurance. Details can be found in the Appendices (Table A2).

2.4.9 SEM-EDX analyses

SEM-EDX analysis was performed to obtain more detailed elemental and morphological information on the soil samples. Secondary Electron and Backscattered Electron images were recorded for carbon-coated sample surfaces using an FEI Quanta 650 FEG environmental scanning electron microscope. One-inch sample holders with soil particles dispersed onto conductive tape were completely scanned by use of backscattered electron detection which results in material contrast images. Particles with high Z elements showed up as bright spots. Chemical analysis by energy dispersive X-ray spectroscopy for selected areas was performed to support the mineral characterization using a Thermo Scientific UltraDry, i.e., Peltier cooled, silicon drift X-ray detector. Data were analyzed by the NORAN System7 microanalysis system, software version 3.3. The primary electron beam energy was 30 keV.

Note that the particles used in our previous study [16] which reported SEM-EDX images and data are from the same overall sample involved different particles with different sizes and are not a part of the results of this report.

2.4.10 XPS analyses

XPS measurements involved a PHI 5000 VersaProbe II (ULVAC-PHI Inc.) system for further investigation of the main soil components. The photoelectrons were generated using monochromatic Al-Kα (1,486.7 eV) radiation as the excitation source, collected at 45° with respect to the surface normal and detected with a hemispherical analyzer. Data analysis was performed using the ULVAC-PHI MultiPak program, version 9.8.

2.5 Extraction procedures

2.5.1 Sequential extraction scheme

Sequential extractions were carried out following a procedure described in previous work focusing on Th,[22] which in turn had been based on a modified version of a sequential extraction scheme also applied to Th.[18] An air-dried mass of approximately 2 g of the original soil sample was used during the extractions for all studied soil types. The five sequential leaching steps are described in Table 1 including the chemicals, duration, pH conditions and target phases. The remaining material (F6) was investigated by (i) direct XRF measurement, as described in Section 2.4.8, on solid residuals after washing and freeze-drying the remainders of F5 solids, and (ii) calculating the differences between total element content (XRF of overall soils) and the sum of the extracted contents from F1 to F5. Fractions F1–F4 targeting metal ions adsorbed at mineral surfaces and bound in secondary phases, are considered to represent non-residual Th in soil, whereas fractions F5 and F6 are supposed to define residual phases, which are not expected to react on short time scales.[18]

Table 1: A summary of the protocol used for the extractions.[22]

Fraction	Target fraction	Extractive reagent at room temperature	pH	Shaking time (h)
F1	Exchangeable	20 mL of 1 mol L^{-1} $MgCl_2$	7	2
F2	Carbonates	30 mL of 1 mol L^{-1} sodium acetate in acetic acid	5	7
F3	Organic matter and/or amorphous oxides	20 mL of 0.1 mol L^{-1} $Na_4P_2O_7$ (pH adjust with 0.1 mol L^{-1} $Na_2H_2PO_4$)	9.8	2
F4	Amorphous Fe–Mn-oxyhydroxides	20 mL of 0.2 mol L^{-1} $(NH_4)_2C_2O_4$ in $H_2C_2O_4$ (Tamm's reagent) in dark	3	5
F5	Crystalline Fe–Mn-oxyhydroxides	20 mL of 0.175 mol L^{-1} sodium citrate in 0.025 mol L^{-1} citric acid (Coffin's reagent)	5	6
F6	Residual	XRF		

After each extraction step, the samples were centrifuged for 10 min at 3,500 rpm. The supernatant from each step was analyzed by Inductively Coupled Plasma Mass Spectrometry (ICP-MS: iCAP TQs, Thermo Scientific). To correct for matrix effects, an internal standard (In-115) was added to each sample prior to analysis. The reference material SPS-SW1, specified for the measurement of elements in surface waters, was used for the quality assurance of ICP-MS measurements. Details of the analytical quality with the detection limits of each trace element analyzed can be found in the Appendices (Table A3). Between each extraction step, the residue was washed with 15 mL Milli-Q water and centrifuged. The supernatants after each washing step were also analyzed by ICP-MS to check for any loss of elements during washing. The chemical compositions of the residual phases were further studied by SEM-EDX. Dilution of the extractants was necessary to keep the salt content below 50 mg L^{-1} in order to avoid clogging of the sample introduction system of the ICP-MS and matrix effects during detection.

Mass balance calculations were performed to compare the sum of the extracted Th in each fraction to the total amount of Th present in the sample. The corresponding total percentage recovery, T_R, was calculated using equation Eq. 5. This verifies the accuracy of the extraction scheme for Th.[22]

$$T_R = \left[\sum_{F_1}^{F_6} M_{S,F} / M_T \right] \times 100 \quad (5)$$

In Eq. 5, $M_{S,F}$ in g is the mass of Th in individual fractions (F1 to F6) while M_T in g is the total mass of Th obtained by XRF.

2.5.2 Single extraction scheme

The same reagents and conditions used during the sequential extractions (except the F6 step) were applied following a single extraction procedure, i.e., parallel extractions.[22] The supernatant from each extraction was analyzed by ICP-MS.

3 Results and discussion

3.1 On-site activity measurements and dose calculations

The activity concentrations of Th-232 and its progenies in all four soil samples are in the range of ~4,000–7,000 Bq kg^{-1}. Even though various factors could contribute to potential errors in these reported activity values during gamma spectroscopic measurements, care was taken to minimize

such errors by following the precautions. Long counting times (72,000 s) were employed to minimize statistical errors. To ensure accurate calibration, the detector energy scale was calibrated using point sources (Cs-137 and Co-60), while efficiency calibration across the full energy range, including high-energy peaks, was performed using an IAEA reference material (Soil-6). Other potential sources of errors include the assumption of secular equilibrium for the U-238 and Th-232 decay series, background radiation subtraction, and variations in sample geometry relative to the calibration standard. To mitigate these factors, samples were sealed for one month to achieve secular equilibrium, and background measurements were periodically conducted to ensure accurate subtraction. The sample geometry was matched to the one for the reference material during calibration. These steps ensured the accuracy and reliability of the NR activities reported in Table 2, which are much higher than for the other NRs detected in the soil samples and higher than the world average for Th-232 content in the soil, which is 30 Bq kg^{-1} (range 11–64 Bq kg^{-1}). The absorbed dose rates 1 m above ground calculated from the radionuclide content of our samples exceed the world average of 57 nGy h^{-1}[11] by more than one order of magnitude (c.f. values in Table 2). Thorium and its progenies are clearly the components in the soil samples with the highest contribution to the background radiation level. Therefore, Th was the primary focus of the present study. According to the UNSCEAR report (2000), absorbed dose rates in the air from monazite-bearing sands in coastal areas of Kerala and Madras range from 200 to 4,000 nGy h^{-1}.[1] The calculated absorbed dose rate values for the Sri Lankan soil samples under study here are higher than in Kerala except for L-03. The significant variations in the measured activity concentrations in locations within a distance of a few meters are somewhat unexpected and suggest local heterogeneity on this scale. The calculated values for the annual effective dose rates due to natural radiation sources (Table 2) are somewhat higher than the world average annual exposure to natural radiation sources of 2.4 mSv yr^{-1} (world range 1–10 mSv yr^{-1}). The differences obtained for effective dose rates calculated using Eq. (4) ($H_{E,C}$) compared to the *in situ* measured values ($H_{E,M}$) using the survey meter (Table 2) may, among other potential causes, be due to the fact that the calculated dose rate is based on the specific contents of a given sample collected at a specific point whereas the on-site measured dose rates include radiation from greater depths and the surroundings. Apparently, the application of Eq. (3) and Eq. (4) rather underestimates the real external dose exposure significantly.

3.2 Laboratory investigations

3.2.1 Physico-chemical characterization of the soil samples

Physico-chemical properties of the collected soil samples are summarized in Table 3. The acidic pH values of 4.4 ± 0.2 and specific surface areas of about 26 ± 4 $m^2 g^{-1}$ of the soil samples are in accordance with the physical properties of other laterite-type soils.[31] The organic contents of the soil samples were found to be moderately high with reference to published total organic carbon (TOC) content classification,[17] which in turn is consistent with the presence of a forest cover on one side of the sample location (Figure 2). Dissolved organic matter is possibly released by rainwater (e.g., during the Monsoon seasons) due to ongoing decomposition and, thus, may contribute to trace metal mobilization.

Table 3: Physicochemical properties of soil samples[a].

Sample	L-03	L-04	L-05	L-06
pH	4.4 ± 0.1	4.2 ± 0.2	4.6 ± 0.4	4.2 ± 0.3
BET surface area ($m^2 g^{-1}$)	28.1 ± 1.3	30.5 ± 1.5	22.7 ± 0.3	21.6 ± 0.3
TOC (g kg^{-1})	1.68 ± 0.01	0.69 ± 0.01	1.77 ± 0.00	1.28 ± 0.01

[a]The results listed are average values of triplicate samples.

Table 2: Activity concentrations, calculated absorbed dose rates, calculated and measured effective dose rates for soil samples.

Sample	K-40[a] (Bq kg^{-1})	Ra-226[a] (Bq kg^{-1})	Th-232[a] (Bq kg^{-1})	Th-232 ($\times 10^{-3}$ mol kg^{-1})	D (nGy h^{-1})	$H_{E,C}$ (mSv yr^{-1})	$H_{E,M}$[b] (mSv yr^{-1})
L-03	340 ± 17	320 ± 80	4,440 ± 365	4.7 ± 0.4	2,928 ± 265	3.6 ± 0.3	36.3 ± 0.1
L-04	530 ± 24	511 ± 106	7,038 ± 647	7.5 ± 0.7	4,642 ± 453	5.7 ± 0.6	28.9 ± 0.4
L-05	539 ± 56	338 ± 109	6,835 ± 639	7.3 ± 0.7	4,436 ± 451	5.4 ± 0.6	12.2 ± 0.1
L-06	462 ± 44	319 ± 89	6,595 ± 880	7.0 ± 0.9	4,275 ± 591	5.2 ± 0.7	9.2 ± 0.2
W_A	400	35	30		57		2.4
W_R[1]	140–850	17–60	11–64		18–93		1–10

D – Calculated absorbed dose rate, $H_{E,C}$ – Calculated effective dose rate, $H_{E,M}$ – measured effective dose rate, W_A – World average, W_R – World range. [a]Errors are from the gamma spectrometry data. [b]Errors are from the readings of three replicates.

3.2.2 Major mineralogy: XRD and ATR-FTIR analyses

XRD patterns obtained for the soil samples studied in this work are shown in Figure 3a along with indications of the main minerals present in the samples. The main XRD reflections agree in the sense that clay minerals and quartz are dominant phases. Other potentially present minerals were not detectable by XRD (i.e., typically, 1–5 wt.% of a mineral are required to be detectable). Another observation is that the color of the soil samples ranges from dark reddish to light reddish, which suggests the presence of Fe (hydr)oxides based on visual inspection of the samples. No reflection was observed for pure Fe containing crystalline phases in any of the diffractograms, probably because the bulk XRD is insensitive to poorly crystalline Fe minerals such as ferrihydrite or to any trace constituents,[39] general low abundance of crystalline Fe phases or due to being predominantly bound to the kaolinite crystal structure. Kaolinite-associated iron oxy-hydroxides, hematite, and goethite are considered the main iron-containing minerals of laterite.[40] The obtained diffractograms for the separated clay fractions are shown in Figure 3b, and exhibit correspondence to kaolinite. Unlike for the spectroscopic investigations applying synchrotron-based X-ray spectroscopies [16] no Th bearing minerals were identified via XRD.

Although it was not a primary objective of this study, an attempt was made to estimate the size of the crystallites. Crystallite size calculations using the Scherrer equation [41] were conducted for quartz using the reflection at approximately 26.64° 2θ. Crystallite sizes of approximately 170 ± 20 nm were obtained from fits to the background subtracted pattern of samples L-03, L-05, and L-06. For sample L-04, the quartz content was insufficient for reliable determination. Because samples were prepared as oriented mounts, the crystallite size determination for kaolinite was not performed due to the strong influence of texture effects on the intensity and full-width-at-half-maximum (FWHM) of reflections for layered compounds.

ATR-FTIR spectra of the soil samples are depicted in Figure 4. The observed bands were assigned based on available literature.[42] Different vibrational fingerprints of clay and silica polymorphs are discernible. The main bands are described here while the remaining band assignments can be found in Figure 4. The O–H stretching at 3,620 cm^{-1} and 3,694 cm^{-1} as well as the deformation bands at 915 cm^{-1} and 938 cm^{-1} are assigned to kaolinite while Si–O stretching at 798 cm^{-1} and 778 cm^{-1} denote the presence of quartz.[42] As with XRD, only the main mineral phases (i.e., kaolinite and quartz) can be identified by this technique because the amounts of other mineral phases were too low to significantly contribute to the spectral features.

3.2.3 Elemental composition: XRF

The amounts of major and trace elements detected in each sample by XRF and their corresponding upper continental crust abundances [43] are shown in Table 4. The results indicate that Si, Al, and Fe dominate the soil matrix, in agreement with the expected dominant oxide phases in Sri Lankan laterite, i.e., Fe_2O_3, Al_2O_3, and SiO_2.[44] The relative abundances of these elements in weight percentages (9–16 wt.%, 25–32 wt.%, and 42–53 wt.%, respectively) agree with those reported by Dahanayake.[44] The amounts of P_2O_5 identified in all samples are in the range of 0.17–0.24 wt.%, comparable to the percentages of REEs and Th in the samples (Table 4). The abundances of the REEs Cerium (Ce), Lanthanum (La), and Neodymium (Nd) are 0.16–0.49 wt.%, 0.09–0.13 wt.% and

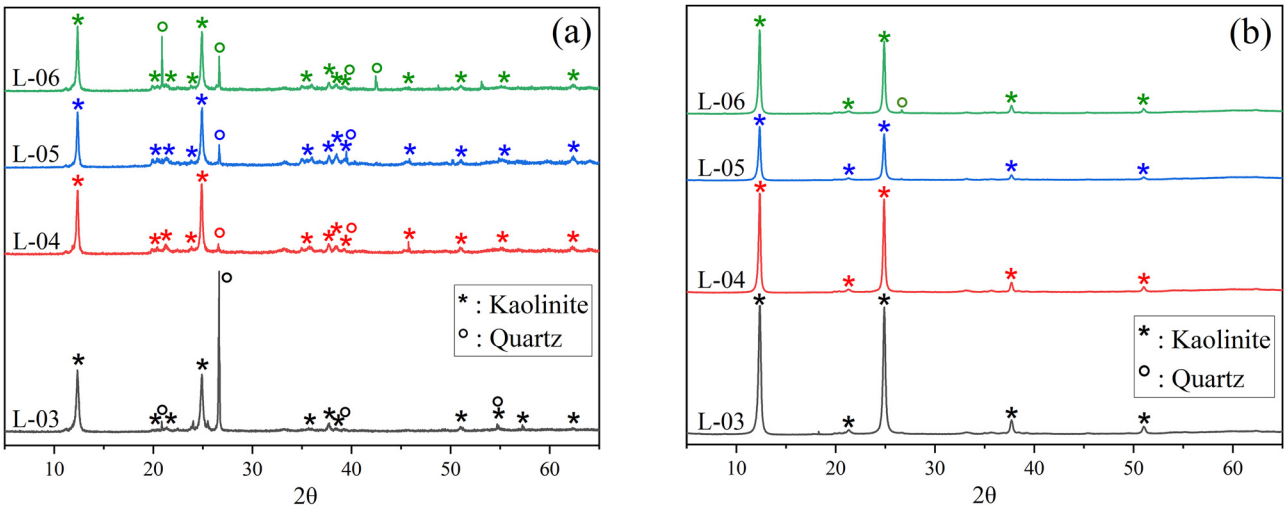

Figure 3: X-ray diffractograms of the samples. (a) Bulk soil and (b) clay fraction separated from the four studied soil samples (L-03 to L-06).

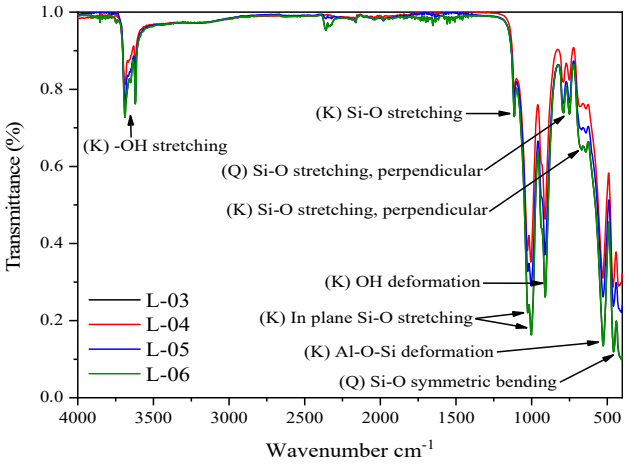

Figure 4: ATR-FTIR spectra of the four soil samples studied. Major components kaolinite (K) and quartz (Q) are indicated by arrows.

0.04–0.06 wt.%, respectively, while Th shows a percentage range from 0.08-0.16 wt.%. Apparently, the contents of those metals are significantly enhanced compared with their average concentration in the upper continental earth crust (UCC) (Table 4).

3.2.4 Surface composition and soil morphology: XPS and SEM-EDX analyses

In order to evaluate mobilization of Th and Lns from those mineral phases and interaction with clay mineral surfaces and secondary phases, more surface specific analyses were performed using XPS and SEM-EDX. XPS (Figure 5, Table 5) and SEM-EDX (Figure 6, Table 6) analyses provide information complementary to XRD results, regarding minor mineral phases and surface composition of the soil particle aggregates. While XRD did not reveal the presence of Th mineral phases, X-ray absorption spectroscopy allowed to quantify Th-phosphate, -oxide and silicate existing in mixed phases.[16] This agreed with SEM-EDX analyses of individual soil grains (Figure 6).

Knowledge about the presence of Fe(III) is important because depending on pH, iron (hydr)oxides are strong sorbents and excellent scavengers for trace elements which makes them another candidate for binding Ln and Th in these soils.[45,46] XPS is rather surface sensitive and the information depth lies in the range of a few nm, so that Th in the sample bulk is not detected. But also surface bound Th in the soil samples will not necessarily be detected by XPS if Th-containing particles in the heterogeneous soil sample with an area of about 0.5 × 0.5 mm^2 are missed by the relatively small electron beam, if the surface bound Th is covered by clay, or if the Th content is simply too low to be detectable.

The XPS analyses clearly identify the presence of iron (in agreement with XRF and SEM-EDX measurements, Figure 6). For example, the obtained amounts in atom-percent by XPS of L-05 are 10.4 % (Al), 14.1 % (Si), and 1.5 % (Fe), respectively, which compares favorably to results obtained by SEM-EDX for the same sample (i.e., 16.6 %, 17.2 %, and 3.2 % for the area in Figure 6a, and 21.9 %, 24.4 %, and 3.7 % for spot analysis in Figure 6b, respectively) as far as the ratios are concerned. This is expected given the fact that both techniques are rather surface-specific compared to the bulk sensitivity of XRF or the XAS methods applied in.[16] At the surface of the soil particles, which means within depths of 2–3 nm, XPS detects Fe(III) only (Figure 5).[47] Unfortunately, Th or REEs could not be identified via XPS analysis due to limited sensitivity, so that an association with Th and Lns cannot be proven.

Even though Th and Ce share some similarities in their chemical and physical properties, the oxidation states of Ce could not be analyzed via XPS in this study because the main lines of Ce, Ce $3d_{5/2}$ and Ce $3d_{3/2}$, located at approximately 884 and 902 eV, were not detected in the spectra, as evident in

Table 4: Concentration of major and trace elements present in the samples measured by XRF.[a]

Sample ID	Major elements			
	SiO_2 (wt.%)	Al_2O_3 (wt.%)	Fe_2O_3 (wt.%)	P_2O_5 ($\times10^{-1}$ wt.%)
L-03	50.2 ± 0.1	24.8 ± 0.6	12.9 ± 0.1	2.4 ± 0.4
L-04	41.4 ± 4.9	31.7 ± 2.2	16.1 ± 0.9	2.1 ± 0.2
L-05	50.7 ± 0.1	24.9 ± 0.2	10.1 ± 0.1	2.4 ± 0.3
L-06	52.8 ± 0.1	26.0 ± 0.3	8.5 ± 0.0	1.7 ± 0.1
UCC[b]	66.6	15.4	5.04	1.5
	Trace elements			
	Ce ($\times10^{-3}$ mol kg^{-1})	La ($\times10^{-3}$ mol kg^{-1})	Nd ($\times10^{-3}$ mol kg^{-1})	Th ($\times10^{-3}$ mol kg^{-1})
L-03	11.5 ± 1.2	9.4 ± 2.8	4.2 ± 1.2	3.4 ± 0.7
L-04	34.7 ± 2.7	6.8 ± 0.2	3.2 ± 0.1	6.4 ± 0.0
L-05	22.2 ± 0.6	8.7 ± 1.0	4.1 ± 0.5	6.7 ± 0.4
L-06	16.2 ± 1.9	6.5 ± 0.6	3.1 ± 0.3	5.5 ± 0.3
UCC[b]	0.45	0.22	0.19	0.05

[a]The results listed are the average value of duplicate samples. [b]Average reported values for the Upper Continental Crust (UCC [43]).

Table 5: Atomic concentrations of elements (at.%) as determined by XPS, relative error ± (10–20) %.

Sample	C	O	Al	Si	Fe
L-03	7.2	67.0	10.0	13.1	2.7
L-04	6.4	67.5	10.7	13.4	2.0
L-05	6.4	67.6	10.4	14.1	1.5
L-06	7.1	67.2	10.3	14.0	1.4

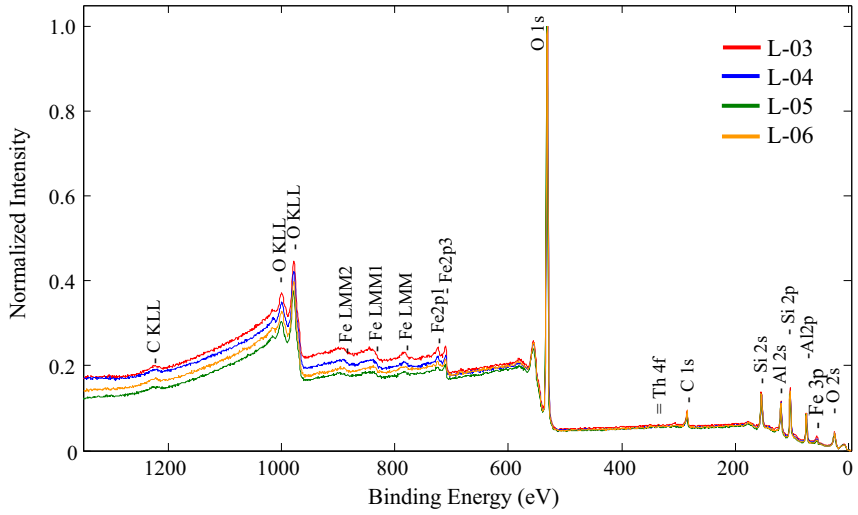

Figure 5: XPS surveys of the soil samples. The positions of the Th 4f main lines are also indicated.

Figure 5. In this binding energy range, survey spectra show an enhanced background due to Fe Auger lines and inelastic scattered photoelectrons from O 1s, which may mask any minor Ce signals. Moreover, XPS spectra were obtained from analysis areas of approximately 500 × 500 μm^2, making detection of Ce challenging due to its low concentration of μm sized Ce containing particles in the sample. For comparison, SEM-EDX analysis of a larger sample area, as shown in Figure 6(a), detected Ce at only 0.02 at.%, which is below the detection limit of XPS.

All soil samples exhibited similar surface characteristics in SEM-EDX analyses, and therefore only a selection is presented in Figure 6a–c. From all SEM-EDX images collected, only those that present phases with the highest Th concentrations are shown (Figure 6d–g). The corresponding percentages (at.%) for the analyzed areas depicted in the SEM images (red squares, Figure 6) are given in Table 6.

The SEM image and the corresponding EDX spectrum from a larger sample area (the area given by the red frame in the inset) are shown in Figure 6a. Different orientations of hexagonal stacking layers of platelike particles are visible in Figure 6b and c. A ratio close to 1:1 of Al: Si atomic concentration in both cases agrees with the presence of kaolinite in the samples inferred from the XRD results (Figure 3b). SEM-EDX in spot-chemical analysis mode yields more conclusive results concerning the local abundance of REE and Th in the soil sample grains.

Concerning Th-bearing minerals, several distinct morphologies were identified. A spherical morphology of Ce-rich minerals containing Th is shown in Figure 6d (25 at.% Ce, 5 at.% Th). The low contents of P and Si in this example (Figure 6d) suggest that Ce and Th occur as an oxide ((Ce, Th)O_2). Literature data provide evidence for (Ce, Th)O_2 solid solutions due to the comparable ionic radii of Th(IV) and Ce(IV).[48] Lanthanum-rich monazite crystals were identified together with kaolinite (Figure 6e), presenting about 18 at.% P and a total of ~13 at.% for La, Ce, Nd, and Th, suggesting that even in close vicinity to clays, these elements are present as phosphates. Kaolinite-associated monazite minerals appear to exhibit a needle-like crystal morphology in our samples. In contrast, an elongated and rectangular Th-rich phosphate mineral (Figure 6f) was observed with ~14 at.% for Th and P, while Si and Al are below 2 at.%. The high amount of P suggests a phosphate phase in which Th occurs without any REEs, atypical for monazite-like phases.

The presence of Th-silicate phases potentially incorporationg a trace amount of Th-phosphate is visible in Figure 6g with 19 at% Th, high at% Si, and low at.% P. The size of the largest Th-silicate mineral identified in one of the samples via SEM is ~200 μm, and Th-REEs containing phosphate minerals are in the size range of 50–250 μm. Thorium associated with the oxide phase (Figure 6h) shows a Th-rich area with 18 at% Th and 77 at% O along with traces of Ce and clay minerals. Unambiguous crystal morphologies cannot be inferred from any of these Th-containing spots in the SEM images.

All these results provide evidence that most of the minerals found in the soil samples are not in pure form but rather present in mixtures of solid phases as earlier reported. [16] Further examples of mixtures involve CeO_2 (crystalline spheres) and (Ce, La, Nd, Th)PO_4 (needle-like crystals), within a single particle (Figure 7).

Overall, three distinct Th-containing phases were identified: Th-oxide, Th-silicate, and Th-phosphate. Unfortunately, unambiguous identification of the respective mineral by SEM-EDX is impossible. Examples of specific Th mineral phases present in nature and in Sri Lankan soils include monazite, thorite, thorianite, uranothorianite, ekanite, allanite, zirkelite, baddeleyite, samarskite, fergusonite,

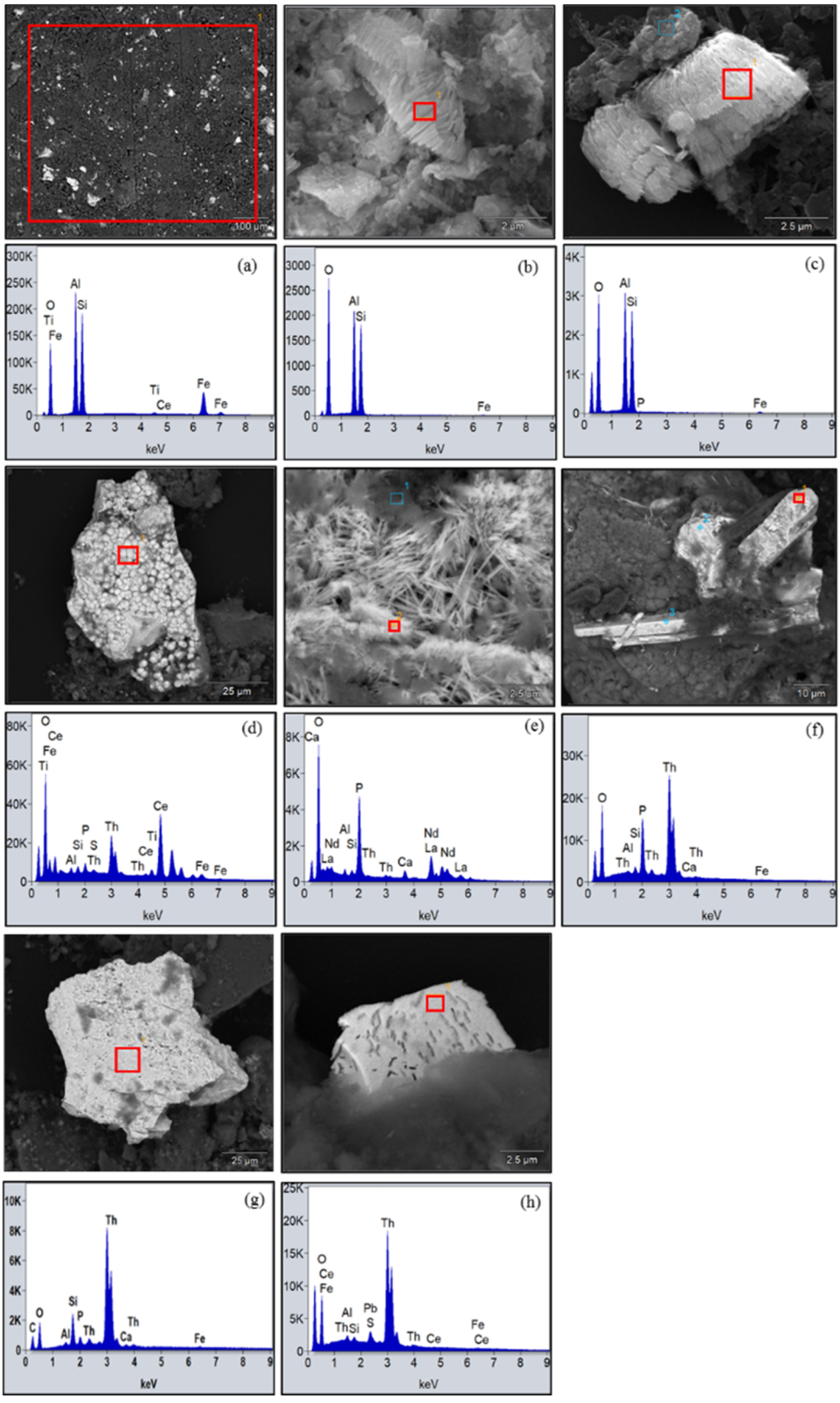

Figure 6: SEM images with corresponding EDX spectra of selected particles from all the soil samples. Particles were selected such that they show the highest content of Th. (a) Area analysis of a sample, (b) and (c) spot analysis of clay minerals which show the hexagonal stacking layers in different orientations; (d) Ce-rich phase; (e) monazite phase; (f) Th-phosphate phase, (g) Th-silicate phase, and (h) Th-oxide phase. Images (b) and (c) were recorded in SE while images (a), (d), (e), (f), (g), and (h) in BSE mode.

Table 6: Atomic concentrations of elements (at. %) in the soil samples from area and spot analysis of Figure 6.

Sample	Element – atom%								
	O–K	Al–K	Si–K	Fe–K	P–K	Ce-L	La-L	Nd-L	Th-M
(a) L-05	62.8 ± 0.5	16.6 ± 0.1	17.2 ± 0.1	3.2 ± 0.0	–	–	–	–	–
(b) L-06	67.4 ± 1.5	15.7 ± 0.5	16.5 ± 0.6	0.4 ± 0.2	–	–	–	–	–
(c) L-06	68.0 ± 1.7	15.1 ± 0.3	16.4 ± 0.5	0.5 ± 0.1	–	–	–	–	–
(d) L-05	59.2 ± 0.6	1.6 ± 0.1	1.9 ± 0.1	2.2 ± 0.2	2.7 ± 0.1	25.2 ± 0.3	–	–	4.6 ± 0.1
(e) L-05	64.3 ± 1.3	1.3 ± 0.3	1.0 ± 0.2	–	18.0 ± 0.3	2.4 ± 0.4	8.6 ± 0.6	2.1 ± 0.5	0.3 ± 0.1
(f) L-05	70.9 ± 1.1	0.5 ± 0.1	1.7 ± 0.1	0.3 ± 0.1	13.8 ± 0.2	–	–	–	13.7 ± 0.2
(g) L-05	62.9 ± 2.5	1.5 ± 0.4	12.5 ± 0.3	0.5 ± 0.3	3.3 ± 0.2	–	–	–	18.6 ± 0.4
(h) L-04	77.0 ± 2.1	1.6 ± 0.3	1.5 ± 0.2	0.5 ± 0.3	–	0.1 ± 0.2	–	–	18.1 ± 0.3

"–" - below the detection limits.

oraganite, bastnaesite, thorogummite, cheralite, zircon, among others.[49,50] Many of these mineral phases are rare and found in mixed forms in nature. For instance, thorianite (ThO_2) and thorite ($ThSiO_4$) crystals are commonly associated with zircon, monazite, and uranite, among others (as observed in this study), and Th can even be incorporated in the zircon structure.[50,51] All in all, the association of Th and REEs to alumosilicates such as kaolinite was not possible to verify by SEM-EDX.

3.2.5 Solid carrier phases of Th and potential mobility: selective extraction approach

The previous results demonstrate that even with surface sensitive spectroscopic investigations it was not possible to identify Th and REE species other than the respective phosphate, oxide or silicate mineral phases. This prompted us to apply selective extraction methods in order to gain further insight into Th and REE speciation. The results of Th extractions for the operationally defined fractions from Table 1 are given in Table 7 as extracted percentages of total Th. Since the main focus of this work is on Th, mainly the results for Th after each extraction step are further discussed, but extracted percentages for La, Ce, and Nd (Table 7) are reported for comparison. The environmental behavior of REEs might be of interest due to their abundance in the investigated soil samples and the current interest in potential exploitation due to their technological importance. The absolute amounts of Th released after extraction steps from both single and sequential procedures are given in the Appendices (Table A4: presenting the extracted Th as dissolved concentration found in the supernatant in Appendices Table A4a and the equivalent results as mass of Th released from the soil samples in Appendices Table A4b).

Before paying closer attention to the results, we emphasize that in general the interpretation of the selective extraction data according to the operationally defined binding modes of trace metals (Table 1) should be considered with caution. Respective assignments are not necessarily specific to a particular metal ion or soil component.[52] Usually, sequential extraction studies regarding radionuclides are performed to assess release of trace amounts in samples from specific, contaminated sites (mines, industrial plants, etc.) into the environment.[22,53] The released radionuclides may interact with soils or sediments primarily via surface interaction (adsorption) or coprecipitation reactions. In the present case, the source for Th is *within* the soil sample. Adding e.g., low pH solutions and/or chelating complexants will dissolve small fractions of

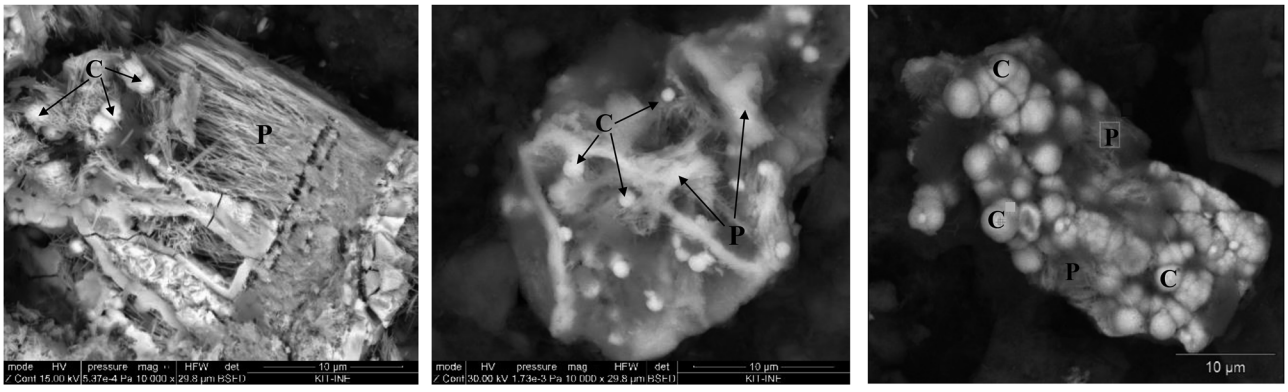

Figure 7: Mixtures of mineral phases in the soil samples. C denotes – (Ce, Th)-oxide phases and P denotes – (Ce, La, Nd, Th)-phosphate phases.

crystalline Th-mineral phases, which then contribute or even dominate the measured Th concentrations in solution. Therefore, as could be expected, the leaching reagents are not necessarily selective for the operationally defined host phases for the trace metals. This becomes obvious for the F2 extraction step, where ideally carbonate mineral bound Th should be dissolved, but such minerals are absent in the acidic lateritic soil.

The overall recovery of Th in the sequential extraction procedure in the present work is in the range of 86–115 % meaning that the sum of the six fractions (i.e., five sequential extractions and direct XRF measurement on F5 residual solids) is in fair agreement with the independent quantification of total Th (i.e., obtained by direct XRF measurements of bulk soil). Furthermore, single and sequential extractions provided similar results for both Th and light REEs (Figure 8), except for extractions of light REEs in fractions F2 and F3, for almost all of the soil samples. Single extractions in these cases show enhanced leaching compared to sequential extractions (Figure 8b–d), consistent with the inherent implications of the procedures. In single extraction steps, the whole original soil is contacted with a given extractant, while it was already leached in the sequential extraction scheme for all fractions except F1. In the sequential scheme, only that fraction can be extracted which is still present after the previous leaching step(s). In the single extraction experiments, leached element fractions may cover multiple fractions of the sequential scheme. The differences in sequential and single extraction experiments become noticeable mainly for the REEs, where relatively large amounts are mobilized in F1, which is not the case for Th (see discussion below). In the single extraction experiments, it seems that this fraction is released in F1 as well as in F2 and, to a lower extent, in F3 and F5.

Collectively, it was observed that Th and the studied REEs in these samples are mainly present in the F6 fraction (Table 7 and Appendices Table A4b). The corresponding percentages for this residual fraction are for Th 69–94 wt.%, La 66–91 wt.%, Ce 71–94 wt.%, and Nd 58–83 wt.%. Guo *et al.* (2007) reported similar results and showed that Th was primarily associated with the residual fraction with

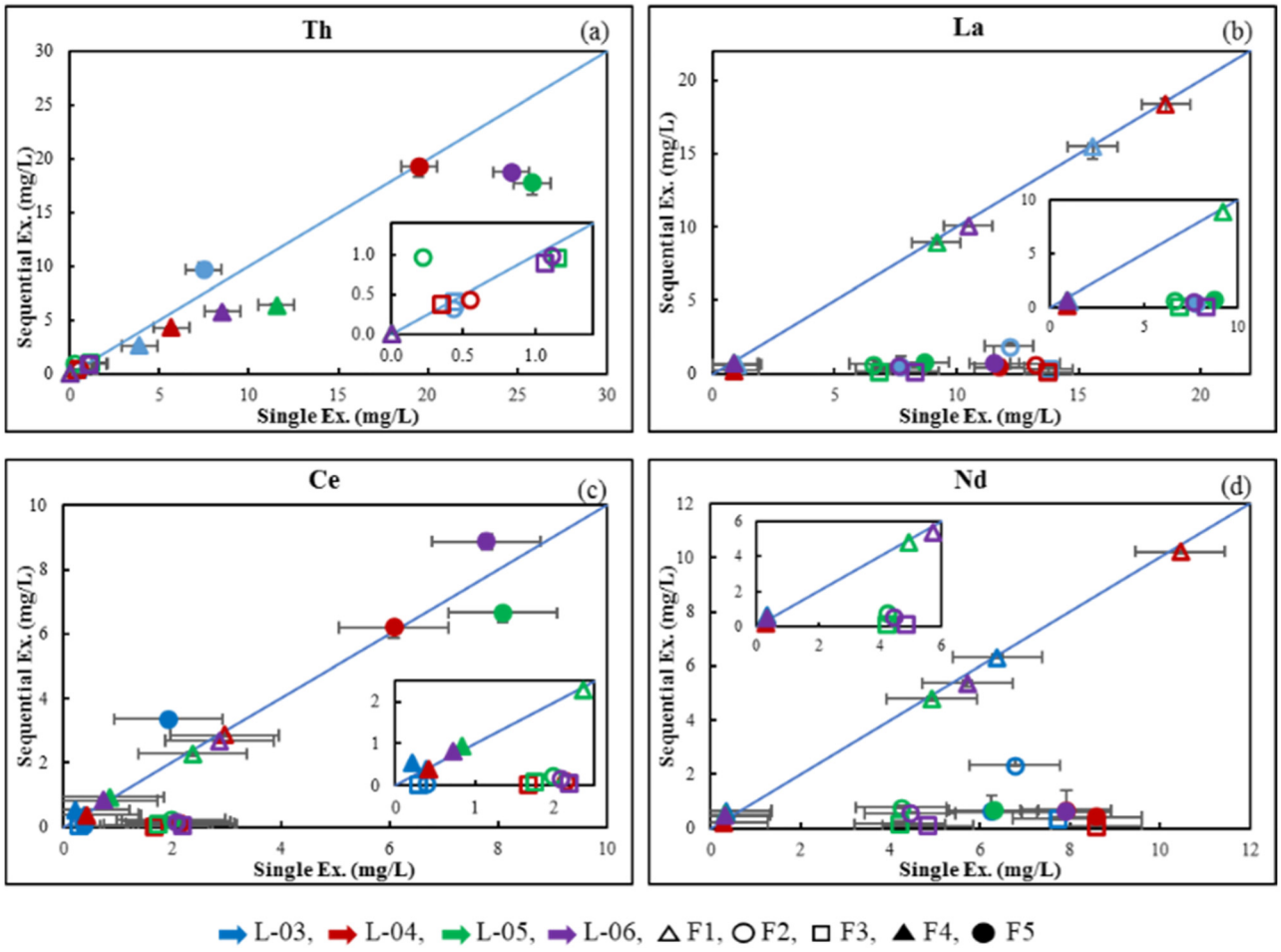

Figure 8: Comparison of sequential and single extractions, for Th and selected REEs in all fractions and four samples. Insets show the fractions for the lower concentrations.

Table 7: Extracted amounts of Th, La, Ce, and Nd in both extraction approaches for all soil samples.

wt.%	Th		La		Ce		Nd	
	Sq	Sn	Sq	Sn	Sq	Sn	Sq	Sn
Overall recovery	82–113		82–105		72–98		81–100	
F1+F2[a]	0.5–1.2	0.6–2.2	8–20	16–40	0.3–1.3	0.6–2.6	10–24	19–48
F3[b]	0.2–0.8		0.1–0.2	6–15	0–1		0–1	7–19
F4[c]	2–5	3–8	0–1		0.1–0.4	0.1–0.3	0.5–1.1	0.5–0.7
F5[d]	6–14	10–16	0.2–0.8	5–10	1–2		0.7–1.3	7–15
F6[e]	69–94		66–91		71–99		58–86	

Sq, Sequential extraction; Sn, Single extraction; a – Easily mobile, b – Organic matter and amorphous oxides, c – Amorphous ferro-manganese oxy(hydroxides), d – Crystalline manganese oxy(hydroxides), e – Residual.

up to 81 % (i.e., after microwave digestion with HF) in samples collected from an REE-related industrial area in Baotou, Inner Mongolia.[22] Martinez-Aguirre and Perianez (2001) also observed ≲70 % of Th in the residual fraction (i.e., obtained by applying approach (ii) described in Section 2.5.1) in samples from a marsh area in southwestern Spain.[54] In an attempt to further understand and identify which soil components associated with Th-minerals are removed by the respective extracting solutions in each step, solid residues sampled after each extraction step were analyzed by SEM-EDX. The results suggest that the main Th mineral phases (i.e., Th-phosphate, Th-silicate, and Th-oxide) do not selectively disappear in any given extraction step. This would be expected for such insoluble phases and supports the hypothesis of reduced mobility of Th in Sri Lankan soils due to its presence in mixtures of solids of low solubility, combined with other elements such as REEs, or dominance of solids presenting crystalline structures.

The experimental results from the extraction schemes suggest that, despite the predominance of identified Th-bearing mineral phases (mainly silicate-, oxide- and phosphate-related), the next highest amount of Th extracted was observed in the (operationally defined) crystalline ferro-manganese oxides and oxyhydroxides (F5) fraction (<20 %, Appendices Table A4). Lower but still important amounts of Th may be present as co-precipitates with amorphous ferro-manganese hydroxides and oxyhydroxides (F4, <8 %, Table 7, Appendices Table A4). The extracted Fe in both F4 and F5 fractions in sequential (i.e., 0.4 ± 0.1 % in F4 and 27 ± 3 % in F5 relative to the overall Fe content) and single extractions (i.e., ~0.2 % in F4 and 17 ± 3 % in F5 relative to the overall Fe content, data not shown) suggest that Fe predominantly occurs in crystalline phases. Respective iron-containing mineral phases, however, could not be identified via bulk soil characterization techniques (see Sections 3.2.2 and 3.2.4), but may be present in lower amounts or exist associated as coatings on other mineral surfaces. Crystalline Fe oxides are rather insoluble but may dissolve under strongly reducing conditions or by microbial activities, releasing trace metals.

The extracted Th amounts of F4 in sequential extraction should be approximately equal to the extracted amounts of F4 minus F1 + F2 in single extraction, but extraction recoveries of F4 are ~ three-fold higher. Thus, because of its low pH (pH~3), the extractant used in F4 may extract F1+F2+F4. Despite the specification that Tamm's oxalate extraction should be conducted in the dark since the oxalate action is light sensitive (Table 1), occasionally, these steps show enhanced extractive power and attack of some crystalline iron oxides, even when carried out in the dark.[55] In fact, Tamm's reagent is characterized by a relatively low pH (pH = 3) and a high concentration of the complexing ligand oxalate. A possible explanation for the relatively high Th concentration in the F4 leachate is the partial dissolution of ThO_2 phases. Solubility control by equilibration with freshly prepared hydrated thorium oxide (solubility concentration: ~0.1 mol L^{-1} at pH = 3 [56]) can be excluded since the concentrations of Th found in the leachate (between 1.1 and 5.0×10^{-5} mol L^{-1}, 2.6–11.5 mg L^{-1}) is higher than the solubility for crystalline ThO_2 phases for the conditions in this work [56] and the solubility of thorium phosphate is even lower.[57] Moreover, the duration of selective extraction steps (a few hours) in our experiments is certainly not sufficient to attain solubility equilibria for hydrated or crystalline ThO_2. Yet, it is clear that ThO_2 will partly dissolve in Tamm's reagent solution.

Results for F3 (extracted Th fraction in both methods at about 1 %, Table 7) suggest minor Th amounts (and also minor REE fractions) being associated with organic matter (OM). A source for the OM content in the soil might be the forest cover in the vicinity of the sampling location, which could continuously supply organic substances to the location. The total organic carbon content (TOC) in soil samples is relatively low (see Table 3). The alkaline (i.e., pH~9.8, Table 1) sodium pyrophosphate solution used in F3 is well-known to solubilize OM and OM-bound metal cations, such as Ca, Mg,

Fe, and Al.[58,59] Interestingly, the study of Kaplan and Serkiz (2001), involving OM contents similar to our samples for soils from a wetland site adjacent to a pilot-scale nuclear facility in South Carolina and involving the same F3 reagent, showed ~65 % extraction of Th [17] whereas Guo *et al.* (2007), again with the same reagent, observed <17 % of Th in F3 from a soil sample with much higher OM content (4–23 g kg^{-1}) [22] compared to our study (<2 g kg^{-1}, Table 4). Those studies indicate that Th could indeed be associated with soil OM. The large variation of Th found in this fraction suggests differences in the chemical speciation of Th in different geological settings and potential differences in the type of OM.

Both the exchangeable fraction (F1) and the carbonate fraction (F2) are susceptible to the F2 single extraction (0.5–2.2 % in both extraction approaches). The F2 fraction is generally considered to involve calcite or aragonite-bound ions, though it is not restricted to this operational definition as many trace elements can be mobilized due to the relatively low pH applied during the extraction (i.e., pH 5). The latter assumption may be valid for Th extraction from Sri Lankan soil (as mentioned before) as no significant carbonate mineral phases were observed in the solid characterization. Measured Th concentrations in the F2 solutions range from 1.4 to 9.7×10^{-6} mol L^{-1} (0.3–2.3 mg L^{-1}) for both extractions, which is somewhat higher than expected in relation to the solubility of freshly prepared hydrated thorium oxide, i.e., 2×10^{-7} mol L^{-1} at pH = 5.[57] The solubility of thorium phosphates (e.g., $Th_3(PO_4)_4$) is expected to be even lower (<10^{-9} mol L^{-1}) under these conditions.[60] Therefore, if the measured Th concentrations arise from the dissolution of a solid phase, the most probable candidate would be thorium oxide (as already discussed before).

Only trace amounts of Th were observed in the exchangeable fraction F1 (single and sequential extractions are obviously identical for this fraction), ranging from 1.7 to 2.6×10^{-8} mol L^{-1} (4–6 µg L^{-1}). The F1 fraction is assumed to represent the ion exchangeable portion released due to the presence of a solution of relatively high ionic strength (i.e., 1 mol L^{-1} $MgCl_2$, Table 1). But in the present case, it seems unlikely that ion exchange between Mg^{2+} and Th^{4+} would explain the obtained results, because Th would rather be specifically and strongly adsorbed. In fact, the pH conditions during F1 extraction (pH ~ 7) combined with the expected low solubility of ThO_2 resulting in concentrations at around 10^{-8} mol L^{-1} for hydrated thorium oxide (~2 µg L^{-1}) [57] are in qualitative accordance with the observations, suggesting that the F1 extraction might as well be influenced by partial ThO_2 dissolution. Since phase separation after the extraction steps is made by centrifugation only, colloidal Th species which are known to form in aqueous solutions, may also contribute to the released Th fractions.

A surprisingly high REE fraction of the soil was leached in F1 and by the washing steps with Milli-Q water (see Appendices Table A5), suggesting that, unlike Th, significant REE amounts are weakly surface bound to clay minerals. This is a clear indication that REE behavior and speciation differs from that of Th. The significant extraction of REEs in F1 and F2 (up to 48 %) clearly points to a relatively weak electrostatic binding to clay minerals. This behavior of REEs is well known for secondary REE sources in weathered crust elution deposited ores, where REEs are adsorbed to clay minerals.[61] From such type of ores, REEs are easily desorbable with inorganic monovalent salt solutions via ionic exchange under mild chemical conditions, which is relevant for REE-mining. Our observation reveals that part of the REEs is much more easily mobilized from REE-Th mineral phases, such as monazite or oxides, than is the case for Th. Released Lns subsequently undergo sorption to clay mineral surfaces. For Th as a tetravalent cation with strong hydrolysis it is well known, that it very strongly binds to oxidic surfaces [62,63] or clay minerals.[64]

Based on our results, less than 9 wt% of Th was estimated to be associated with non-residual fractions due to nominal solid host phase dissolution (i.e., the sum of the sequentially extracted amounts in F1, F2, F3, and F4 or the single F4 extraction), which reflects potential mobility in the environment under certain conditions. For instance, environmental processes involving degradation/dissolution of OM and amorphous Fe/Mn mineral phases via remineralization or early diagenesis [65–67] may play a role in transferring a relatively small fraction of natural Th (i.e., max. 9 wt.% of the total Th content, representing ~115 mg kg^{-1}) into the environment. This, however, is only relevant under the assumption that Th is indeed bound to OM and amorphous Fe/Mn mineral phases. Other relatively mild environmental perturbations taking place throughout the hydrological cycle (i.e., interaction between rocks and plants during water runoff, percolation, underground water, (acid) rain, infiltration surface water and groundwater, etc.) may lead, to some extent, to similar Th mobility.[53] One also has to take into account that lateritic soil porewaters are relatively acidic, thereby enhancing solubility of e.g., ThO_2 as discussed before. Therefore, one should also verify the geochemical behavior of dissolved Th because its environmental dispersion/transport may finally be linked to commonly present colloidal carrier phases including organic matter (present as a moderate amount in the studied soils, Table 3) or amorphous Fe/Mn oxyhydroxides.[68] It is also to be expected that, on the way to the groundwater concomitant with increasing pH, sorption phenomena will decrease metal ions concentrations and notably Th concentrations in solution (e.g.,

silica, hematite, and clay mineral surfaces, among others, bare or covered with organic matter such as fulvic and humic acids [63,69,70]). Evaluation of the effective mobility of Th, thus, needs to consider those processes, which can be investigated e.g., by column leaching experiments with simulated rainwater. Our results highlight the need for comprehensive studies including several environmental compartments to better understand the environmental dispersion, fate, and impact of NRs for risk assessment purposes.

The speciation of thorium discussed in this study, particularly in relation to its mobility and association with certain mineral phases, has broader implications for understanding radioactive hazards in other geologic environments. In inland regions characterized by igneous rocks such as granite, or volcanic terrains, naturally occurring Th can be present at elevated levels.[71,72] These environments may exhibit similar speciation patterns, where Th is largely immobile and strongly adsorbed to refractory minerals like kaolinite or present in insoluble phases. Understanding the speciation of Th in these settings is crucial for assessing potential radioactive hazards, as the mobility/bioavailability of Th can impact long-term environmental and human health risks. In this sense, insights from this study could help inform management practices in mining areas or regions where thorium-bearing minerals occur, contributing to the broader field of environmental radioactivity and geochemical modelling.

4 Conclusions

Soil samples from a playground located in central Sri Lanka were characterized using different techniques. The potential mobility of elements such as radioactive nuclides (natural Th-232) and metal ions of potential economic interest (light REEs) was tentatively quantified with selective extraction techniques. The results suggest that Th-containing mineral phases exhibit a broad variability and a surprising heterogeneity given the small sampling area of the present study. As one major observation, the school playground exhibits significant radiation dominated by Th and progenies. From the geochemical analysis, it was concluded in agreement with earlier investigations that Th and REE occur together as well as separately in silicate, oxide, and phosphate (probably monazite-type) phases. Such phases comprise ~0.2 wt.% of Th in these soils, which are dominated by clay minerals and quartz, with iron phases present in low amounts (<5 wt.%). Selective extractions suggest that the largest fraction of Th is associated with the residual fraction (69–94 wt.%). Less than 9 wt.% of Th of total Th content was retrieved in the chemical extraction steps, reflecting the upper limit of the potential mobility in the environment under specific conditions. The naturally low pH of the lateritic soil may play a role in Th mobilization due to enhanced solubility of Th-containing mineral phases, mainly iron oxides, and ThO_2. Mobilization and subsequent transport to the groundwater need to be addressed and the role of colloidal species should be studied indeed in future investigations.

Overall, our results suggest that radiological exposure to humans (contributing most of the elevated radiation levels in the location of interest, Sri Lanka) is expected to be strongly associated with the radiation from Th-232 and its progenies in small mineral particles that we expected to be relatively stable and immobile. Therefore, maximum exposure will most probably arise from *in situ* external radiation and inhalation of dust particles, especially during dry seasons, and become particularly relevant in places such as a school playground. Further research should focus on the radiological hazard on humans from long-term exposure to *in situ*, naturally radioactive environments and on the development of appropriate management measures when applicable.

Acknowledgements: We are grateful for the support by the Analytical group of KIT-INE and Ms. Beate Oetzel and Dr. Utz Kramar for XRF analysis at AGW-KIT. SR thanks the staff of SLAEB and Mr. U. De Silva from GSMB for their kind support throughout this project and during sampling. Mr. Nirmala Wickramasinghe and Mr. Dilshan Bandara are acknowledged for their support during sampling and geological surveys, and Ms. Rukshagini Pathmanathan for analytical help in Sri Lanka (National Institute of Fundamental Studies, Sri Lanka).
Research ethics: Not applicable.
Informed consent: Not applicable.
Author contributions: All authors have accepted responsibility for the entire content of this manuscript and approved its submission.
Use of Large Language Models, AI and Machine Learning Tools: None declared.
Conflict of interest: The authors state no conflict of interest.
Research funding: This work was supported by the DAAD – German Academic Exchange Service under the Research Grant – Doctoral Programs in Germany, 2017/18 (Grant number 57299294). Some of the fieldwork in Sri Lanka was covered by a grant from the National Research Council of Sri Lanka (NRC 16-015).
Data availability: Data available on request from the authors.

Appendices

See tables Tables A1–A5

Table A1: Radionuclides with the energy of gamma ray.

Parent radionuclide	Daughters	Energy (keV)	Abundance P_γ[a] (%)
Th-232	Pb-212	238.63	43.20
	Ac-228	338.32	11.27
		911.23	25.80
		968.97	15.80
	Tl-208	583.19	30.37
Ra-226	Ra-226	186.10	3.50
	Pb-214	295.22	19.30
		351.93	37.60
	Bi-214	609.31	46.10
		1,120.29	15.10
		1,764.49	15.10
K-40	K-40	1,460.81	10.67

[a]P_γ is the absolute transition probability.

Table A2: Analytical quality assurance of the ED-XRF measurements.

	La	Ce	Th	Nd
Sy-3-M	1,340 ± 11	2,267 ± 21	1,019 ± 8	649 ± 3
Sy-3-S	1,317 ± 20	2,251 ± 20	904 ± 10	796 ± 10
Accuracy (%)	100 ± 1	102 ± 1	102 ± 1	97 ± 0
Sy-2-M	70 ± 1	174 ± 6	402 ± 7	76 ± 4
Sy-2-S	77 ± 5	161 ± 10	386 ± 10	77 ± 5
Accuracy (%)	94 ± 2	99 ± 3	106 ± 2	104 ± 6
BE-N-M	92 ± 1	180 ± 4	17 ± 1	74 ± 6
BE-N-S	82 ± 5	153 ± 10	11 ± 5	66 ± 5
Accuracy (%)	113 ± 2	118 ± 3	163 ± 7	111 ± 9

[a]M measured value, S – standard value. All the analysed elements were checked with certified reference materials of rock samples (units are in mg kg^{-1}).

Table A3: Averaged results from analytical quality of the ICP-MS measurements.

	La	Ce	Th	Nd
SPS-SW1-M	503 ± 6	496 ± 18	519 ± 19	504 ± 16
SPS-SW1-S	500 ± 10	500 ± 10	500 ± 10	500 ± 10
Accuracy (%)	101 ± 1	99 ± 4	104 ± 4	101 ± 3
Detection limit	0.04–0.14	0.06–0.14	0.04–0.10	0.07–0.13

[a]M measured value, S – standard value. The analysed trace elements were checked with certified reference material of SPS-SW1 and detection limits (units are in ng L^{-1}).

Table A4: (a) Amount of Th extracted in sequential (Sq) and single (Sin) extractions.

	F1 (µg L^{-1})		F2 (µg L^{-1})		F3 (µg L^{-1})		F4 (mg L^{-1})		F5 (mg L^{-1})	
	Sq	Sin	Sq	Sin	Sq	Sin	Sq	Sin	Sq	Sin
L-03	4.45 ± 1.91	4.46 ± 0.33	330 ± 5	433 ± 6	402 ± 12	438 ± 1	2.58 ± 0.03	3.88 ± 0.07	9.63 ± 0.23	7.13 ± 0.45
L-04	6.11 ± 1.40	5.80 ± 1.25	445 ± 8	542 ± 29	372 ± 20	350 ± 6	4.28 ± 0.07	5.68 ± 0.02	19.8 ± 0.4	19.4 ± 0.0
L-05	3.51 ± 0.59	4.85 ± 1.31	977 ± 21	2,236 ± 17	960 ± 31	1,160 ± 33	6.38 ± 0.01	11.5 ± 0.1	17.1 ± 0.5	25.8 ± 0.1
L-06	4.40 ± 1.36	4.65 ± 1.65	988 ± 1	1,115 ± 9	897 ± 4	1,060 ± 8	5.78 ± 0.01	8.54 ± 0.08	18.6 ± 0.3	24.7 ± 0.1

Table A4: (b) Amount of Th extracted in sequential (Sq) and single (Sin) extractions; mass of Th released from the soil.

	F1 (ng g^{-1})		F2 (µg g^{-1})		F3 (µg g^{-1})		F4 (µg g^{-1})		F5 (µg g^{-1})		F6 (mg kg^{-1})	Total (mg kg^{-1})
	Sq	Sin	Sq	Sin	Sq	Sin	Sq	Sin	Sq	Sin	Sq	
L-03	44.5 ± 19.1	44.6 ± 3.3	4.94 ± 0.01	6.49 ± 0.09	4.02 ± 0.12	4.38 ± 0.01	25.8 ± 0.3	38.8 ± 0.7	96.3 ± 2.3	71.3 ± 4.5	656 ± 5	794 ± 162
L-04	61.1 ± 14.0	58.0 ± 12.5	6.68 ± 0.11	8.13 ± 0.44	3.72 ± 0.20	3.50 ± 0.05	42.8 ± 0.7	56.7 ± 0.2	198 ± 4	193 ± 1	1,020 ± 149	1,480 ± 5
L-05	35.1 ± 5.9	39.3 ± 0.0	14.6 ± 0.3	33.5 ± 0.26	9.60 ± 0.31	11.6 ± 0.3	63.8 ± 0.1	115 ± 1	172 ± 5	258 ± 1	1,150 ± 99	1,560 ± 98
L-06	44.0 ± 13.6	46.5 ± 16.5	14.8 ± 0.0	16.7 ± 0.1	8.97 ± 0.04	10.6 ± 0.1	57.8 ± 0.1	85.4 ± 0.8	186 ± 3	247 ± 1	1,200 ± 132	1,280 ± 76

Table A5: Released amounts of elements of interests in the washing steps between each sequential extraction.

	F1 (mg L^{-1})	F2 (µg L^{-1})	F3	F4	F5
Th			(mg L^{-1})	(mg L^{-1})	(mg L^{-1})
L-04	<	16.9 ± 2.9	1.5 ± 0.0	0.3 ± 0.0	1.6 ± 0.0
L-05	<	8.7 ± 2.6	1.6 ± 0.0	0.2 ± 0.0	1.5 ± 0.0
U			(µg L^{-1})	(µg L^{-1})	(µg L^{-1})
L-04	<	7.6 ± 0.2	23.5 ± 0.0	16.5 ± 0.4	23.5 ± 0.0
L-05	<	<	19.3 ± 0.5	7.0 ± 0.1	19.3 ± 0.5
La			(mg L^{-1})		(mg L^{-1})
L-04	1.7 ± 0.3	40.4 ± 2.2	0.6 ± 0.0	15.0 ± 1.2	0.6 ± 0.0
L-05	0.7 ± 0.1	14.3 ± 1.1	0.4 ± 0.0	11.7 ± 0.2	0.4 ± 0.0
Ce					
L-04	0.3 ± 0.0	11.0 ± 1.4	2.3 ± 0.0	34.4 ± 0.7	2.3 ± 0.0
L-05	0.3 ± 0.0	10.4 ± 0.5	1.9 ± 0.0	33.7 ± 1.6	1.9 ± 0.0
Nd					
L-04	1.1 ± 0.1	39.9 ± 2.0	0.3 ± 0.0	14.6 ± 0.7	0.3 ± 0.0
L-05	0.4 ± 0.1	16.1 ± 0.0	0.2 ± 0.0	12.2 ± 2.7	0.2 ± 0.0

***** "<" - below the detection limit. Data only for Th, U, La, Ce, and Nd per gram of soil (L-04 and L-05) are given in this table.

References

1. UNSCEAR: *Sources and Effects of Ionizing Radiation*; United Nations: New York, 2000. https://www.unscear.org/docs/publications/2000/UNSCEAR_2000_Report_Vol.I.pdf (accessed 2019-05-08).
2. Von Gunten, H. R.; Beneš, P. Speciation of Radionuclides in the Environment. *Radiochim. Acta* **1995**, *69*, 1–30.
3. Nalaka, D. S.; Prasad, M.; Nimalsiri, T. B.; Suriyaarchchi, N. B.; Iimoto, T.; Ishikawa, T.; Omori, Y.; Dissanayake, C. B. Measuring Radon and Thoron Levels in Sri Lanka. *Adv. Mat. Res.* **2013**, *718–720*, 721–724.
4. Herath, M. M. J. W. *Beach Mineral Sands in Sri Lanka. Occurrence, Global Trends, and Current Issues*; Geological Survey and Mines Bureau: Colombo, Sri Lanka, 2008.
5. Ismail, M. G. M. U.; Amarasekera, J.; Kumarasinghe, J. S. N. The Upgrading of Ilmenite from Sri Lanka by the Oxidation-Reduction-Leach Process. *Int. J. Miner. Process.* **1983**, *10* (2), 161–164.
6. Wickremeratne, W. S. Preliminary Studies on the Offshore Occurrences of Monazite-Bearing Heavy-Mineral Placers, Southwestern Sri Lanka. *Mar. Geol.* **1986**, *72*, 1–9.
7. Pram, W.; Pohl, J. Geochemistry of Pelitic and Psammopelitic Precambrian Metasediments from Southwestern Sri Lanka: Implications for Two Contrasting Source-Terrains and Tectonic Settings. *Precambrian Res*. **1994**, *66* (1–4), 223–244.
8. Rupasinghe, M. S.; Dissanayake, C. B. The Rare-Earth Element Abundance in the Sedimentary Gem Deposits of Sri Lanka. *Lithos* **1984**, *17*, 329–342.
9. Warnakulasuriya, T.; Williams, S.; Weerakkody, T.; Dabarera, M.; Rodrigo, K.; Waduge, V. A.; Ediriweera, D.; Siriwardena, N.; Wickremasinghe, R. Background Radiation Levels Near a Mineral

Sand Mining Factory in Sri Lanka: Correlation of Radiation Measurements with Micronuclei Frequency. *Radiat. Prot. Dosim.* **2020**, *189* (1), 114–126.
10. Mahawatte, P.; Fernando, K. Radioactivity Levels in Beach Sand from the West Coast of Sri Lanka. *J. Natl. Sci. Found. Sri Lanka* **2013**, *41* (4), 279–285.
11. SLAEB. *Annual Report*; Sri Lanka Atomic Energy Board: Colombo, 2015. https://aeb.gov.lk/wp-content/uploads/2020/12/3.Annual-Report-2015-English.pdf (accessed 2019-05-02).
12. *Baseline Radioactivity Data*: Sri Lanka Atomic Energy Board: Colombo. https://aeb.gov.lk/soil/ (accessed 2017-10-10).
13. ICRP Publication 103: The 2007 Recommendations of the International Commission on Radiological Protection. *Ann. ICRP* **2007**, *37*(2–4).
14. EPA: *Thorium*; United States Environmental Protection Agency, 2017. https://semspub.epa.gov/work/HQ/175255.pdf (accessed 2019-06-11).
15. ATSDR. *Toxicological Profile for Thorium*; U.S. Department of Health and Human Services: Georgia, 1990. https://www.atsdr.cdc.gov/ToxProfiles/tp147.pdf (accessed 2019-06-11).
16. Ratnayake, S.; Lützenkirchen, J.; Finck, N.; Schild, D.; Heberling, F.; Gil-Díaz, T.; Dardenne, K.; Rothe, J.; Geckeis, H. Combined X-Ray Absorption and SEM–EDX Spectroscopic Analysis for the Speciation of Thorium in Soil. *Sci. Rep.* **2023**, *13*, 5877.
17. Kaplan, D.; Serkiz, S. Quantification of Thorium and Uranium Sorption to Contaminated Sediments. *J. Radioanal. Nucl. Chem.* **2001**, *248*, 529–535.
18. Martinez-Aguirre, A.; Garcia-León, M.; Ivanovich, M. U and Th Speciation in River Sediments. *Sci. Total Environ.* **1995**, *173–174*, 203–209.
19. Strok, M.; Smodis, B. Comparison of Two Sequential Extraction Protocols for Fractionation of Natural Radionuclides in Soil Samples. *Radiochim. Acta* **2010**, *98* (4), 221–229.
20. Tessier, A.; Campbell, P. G. C.; Bisson, M. Sequential Extraction Procedure for the Speciation of Particulate Trace Metals. *Anal. Chem.* **1979**, *51* (7), 844–851.
21. Barreto, S. R. G.; Nozaki, J.; De Oliveira, E.; Do Nascimento Filho, V. F.; Aragão, P. H. A.; Scarminio, I. S.; Barreto, W. J. Comparison of Metal Analysis in Sediments Using EDXRF and ICP-OES with the HCl and Tessie Extraction Methods. *Talanta* **2004**, *64* (2), 345–354.
22. Guo, P.; Duan, T.; Song, X.; Chen, H. Evaluation of a Sequential Extraction for the Speciation of Thorium in Soils from Baotou Area, Inner Mongolia. *Talanta* **2007**, *71* (2), 778–783.
23. Tack, F. M. G.; Vossius, H. A. H.; Verloo, M. G. A Comparison between Sediment Fractions, Obtained from Sequential Extraction and Estimated from Single Extractions. *Int. J. Environ. Anal. Chem.* **1996**, *63* (1), 61–66.
24. Silva, E. I. L.; Manuweera, L. Surface and Rainwater Chemistry in Sri Lanka–A Risk of Acidification. *Asian J. Water, Environ. Pollut.* **2004**, *1* (1–2), 79–86.
25. Fernando, G. W. A. R.; Pitawala, A.; Amaraweera, T. H. N. G. Emplacement and Evolution History of Pegmatites and Hydrothermal Deposits, Matale District, Sri Lanka. *Int. J. Geosci.* **2011**, *2*, 348–362.
26. Dharnapriya, P. L.; Malaviarachchi, S. P. K.; Kriegsman, L. M.; Galli, A.; Dyck, B.; Sajeev, K.; Su, B.; Pitawala, A. Symplectite Growth in the Presence of Alkaline Fluids: Evidence from Hugh-Aluminous Metasediments of the Highland Complex, Sri Lanka. *Mineral. Petrol.* **2020**, *114*, 515–538.
27. Ningappa, C.; Sannappa, J.; Karunakara, N. Study on Radionuclides in Granite Quarries of Bangalore Rural District, Karnataka, India. *Radiat. Prot. Dosim.* **2008**, *131* (4), 495–502.
28. Lokesh, N.; Vinutha, P. R.; Malleshi, K.; Narayana, Y. Natural Radionuclides in Rocks and Their Association with the Mineralogy of Rocks in Dakshina Kannada Region of Southern India. *Acta Geophys* **2022**, *70*, 2149–2160.
29. Iqbal, M.; Tufail, M.; Mirza, S. M. Measurements of Radioactivity in Marble Found in Pakistan Using a NaI(Tl) Gamma-Ray Spectrometer. *J. Environ. Radioact.* **2000**, *51* (2), 255–265.
30. Uosif, M. A. M.; Abdel-Salam, L. M. An Assessment of the External Radiological Impact in Granites and Pegmatite in Central Eastern Desert in Egypt with Elevated Natural Radioactivity. *Radiat. Prot. Dosimetry* **2011**, *147* (3), 467–473.
31. Ranasinghe, R.; Werellagama, D.; Weerasooriya, R. Arsenite Removal from Drinking Water Using Naturally Available Laterite in Sri Lanka. *Eng. J. Inst. Eng. Sri Lanka* **2014**, *47* (2), 23–31.
32. FAO: *Acid Soils* **2019**. https://www.fao.org/soils-portal/soil-management/management-of-some-problem-soils/acid-soils/en/ (accessed 2019-07-20).
33. Salminen, R.; Batista, M. J.; Bidovec, M.; Demetriades, A.; De Vivo, B.; De Vos, W.; Duris, M.; Gilucis, A.; Gregorauskiene, V.; Halavic, J.; Heitzmann, P. *Geochemical atlas of Europe. Part 1, Background Information, Methodology, and Maps*; Geological Survey of Finland: Espoo, 2005. http://weppi.gtk.fi/publ/foregsatlas/maps_table.php (accessed 2019-07-07).
34. IAEA-TECDOC-1415. *Soil Sampling for Environmental Contaminant*; International Atomic Energy Agency: Vienna, 2004. https://www-pub.iaea.org/MTCD/Publications/PDF/te_1415_web.pdf (accessed 2017-10-01).
35. IAEA *Measurement of Radionuclides in Food and the Environment. Technical Report Series No. 295*; International Atomic Energy Agency: Vienna, 1989. https://inis.iaea.org/collection/NCLCollectionStore/_Public/20/041/20041399.pdf (accessed 2010-10-15).
36. Beck, H. L.; Decampo, J.; Gogolak, C. *In Situ Ge (Li) and NaI (Tl) Gamma-Ray Spectrometry*; Technical Report, United States Atomic Energy Commission: New York, 1972. https://www.osti.gov/servlets/purl/4599415.
37. Carter, M. R.; Gregorich, E. G. *Soil Sampling and Methods of Analysis*, 2nd ed.; CRC Press: Florida, 2007.
38. Estefan, G.; Rolf, S.; John, R., Eds. In *Methods of Soil, Plant, and Water Analysis: A Manual for the West Asia and North Africa Region*, 3rd ed.; ICRDA: Lebanon, 2013.
39. Johnston, J. H.; Lewis, D. G. A Detailed Study of the Transformation of Ferrihydrite to Hematite in an Aqueous Medium at 92°C. *Geochim. Cosmochim. Acta* **1983**, *47* (11), 1823–1831.
40. Boudeulle, M.; Muller, J.-P. Structural Characteristics of Hematite and Goethite and Their Relationships with Kaolinite in a Laterite from Cameroon. A TEM Study. *Bull. Minéral.* **1988**, *111* (2), 149–166.
41. Holzwarth, U.; Gibson, N. The Scherrer Equation versus the 'Deby-Scherrer Equation. *Nat. Nanotechnol.* **2011**, *6*, 534.
42. Madejova, J.; Komadel, P. Baseline Studies of the Clay Minerals Society Source Clays: Infrared Methods. *Clays Clay Miner.* **2001**, *49*, 410–432.
43. Rudnick, R. L.; Gao, S. Composition of the Continental Crust. In *Treatise on Geochemistry*; Holland, HD.; Turekian, K. K., Eds.; Elsevier: Netherlands, Vol. 3, 2003; pp. 1–64.
44. Dahanayake, K. Laterites of Sri Lanka – A Reconnaissance Study. *Miner. Depos.* **1982**, *17*, 245–256.
45. Musić, S.; Ristić, M. Adsorption of Trace Elements or Radionuclides on Hydrous Iron Oxides. *J. Radioanal. Nucl. Chem.* **1988**, *120*, 289–304.
46. Rojo, I.; Seco, F.; Rovira, M.; Giménez, J.; Cervantes, G.; Martí, V.; De Pablo, J. Thorium Sorption onto Magnetite and Ferrihydrite in Acidic Conditions. *J. Nucl. Mater.* **2009**, *385* (2), 474–478.

47. Seyama, H.; Soma, M. Fe 2p Spectra of Silicate Minerals. *J. Electron Spectros. Relat. Phenomena* **1987**, *42* (1), 97–101.
48. Shannon, R. D. Revised Effective Ionic Radii and Systematic Studies of Interatomic Distances in Halides and Chalcogenides. *Acta Cryst. A* **1976**, *32*, 751–767.
49. René, M. Nature, Sources, Resources, and Production of Thorium. In *Descriptive Inorganic Chemistry Researches of Metal Compounds*; Akitsu, T., Ed.; IntechOpen: London, 2017. https://www.intechopen.com/chapters/54850.
50. Tennakone, K. Thorium Minerals in Sri Lanka, History of Radioactivity and Thorium as a Future Energy Source: a Compendium to Commemorate the International Year of Chemistry 2011. *J. Natl. Sci. Found. Sri Lanka* **2011**, *39* (2), 97–111.
51. Langmuir, D.; Herman, J. S. The Mobility of Thorium in Natural Waters at Low Temperatures. *Geochim. Cosmochim. Acta* **1980**, *44* (11), 1753–1766.
52. Du Bray, E. A., Ed. In *Preliminary compilation of descriptive geoenvironmental mineral deposit models*; U.S. Geological Survey: Denver, Colorado, 1995.
53. Bednar, A. J.; Gent, D. B.; Gilmore, J. R.; Sturgis, T. C.; Larson, S. L. Mechanisms of Thorium Migration in a Semiarid Soil. *J. Environ. Qual.* **2004**, *33* (6), 2070–2077.
54. Martínez-Aguirre, A.; Perianez, R. Sedimentary Speciation of U and Th Isotopes in a Marsh Area at the Southwest of Spain. *J. Radioanal. Nucl. Chem.* **2001**, *247*, 45–52.
55. Gleyzes, C.; Tellier, S.; Astruc, M. Fractionation Studies of Trace Elements in Contaminated Soils and Sediments: a Review of Sequential Extraction Procedures. *TrAC-Trends Anal. Chem.* **2002**, *21* (6-7), 451–467.
56. Neck, V.; Altmaier, M.; Müller, R.; Bauer, A.; Fanghänel, T.; Kim, J.-I. Solubility of Crystalline Thorium Dioxide. *Radiochim. Acta* **2003**, *91*, 253–262.
57. OECD/NEA. *Chemical Thermodynamics of Thorium. Chemical Thermodynamics*; OECD Publishing: Paris, 2008; p. 11.
58. Fox, P. M.; Nico, P. S.; Tfaily, M. M.; Heckman, K.; Davis, J. A. Characterization of Natural Organic Matter in Low-Carbon Sediments: Extraction and Analytical Approaches. *Org. Geochem.* **2017**, *114*, 12–22.
59. Lopez-Sangil, L.; Rovira, P. Sequential Chemical Extractions of the Mineral-Associated Soil Organic Matter: An Integrated Approach for the Fractionation of Organo-Mineral Complexes. *Soil Biol. Biochem.* **2013**, *62*, 57–67.
60. Rai, D.; Yui, M.; Kitamura, A.; Grambow, B. Thermodynamic Approach for Predicting Actinide and Rare Earth Concentrations in Leachates from Radioactive Waste Glasses. *J. Solution Chem*. **2011**, *40*, 1473–1504.
61. Moldoveanu, G. A.; Papangelakis, V. G. Leaching of Lanthanides from Various Weathered Elution Deposited Ores. *Can. Metall. Q.* **2013**, *52* (3), 257–264.
62. Cromières, L.; Moulin, V.; Fourest, B.; Guillaumont, R.; Giffaut, E. Sorption of Thorium onto Hematite Colloids. *Radiochim. Acta* **1998**, *82*, 249–256.
63. Östhols, E. Thorium Sorption on Amorphous Silica. *Geochim. Cosmochim. Acta* **1995**, *59* (7), 1235–1249.
64. Bradbury, M. H.; Baeyens, B. Sorption Modelling on Illite. Part II: Actinide Sorption and Linear Free Energy Relationships. *Geochim. Cosmochim. Acta* **2009**, *73* (4), 1001–1013.
65. Dahanayake, K.; Subasinghe, S. A Modern Terrestrial Phosphorite-An Example from Sri Lanka. *Sediment. Geol.* **1989**, *61* (3–4), 311–316.
66. Driese, S. G.; Medaris, L. G. Jr.; Ren, M.; Runkel, A. C.; Langford, R. P. Differentiating Pedogenesis from Diagenesis in Early Terrestrial Paleoweathering Surfaces Formed on Granitic Composition Parent Materials. *J. Geol.* **2007**, *115*, 387–406.
67. Froelich, P.; Klinkhammer, G. P.; Bender, M. L.; Luedtke, N. A.; Heath, G. R.; Cullen, D.; Dauphin, P.; Hammond, D.; Hartman, B.; Maynard, V. Early Oxidation of Organic Matter in Pelagic Sediments of the Eastern Equatorial Atlantic: Suboxic Diagenesis. *Geochim. Cosmochim. Acta* **1979**, *43* (7), 1075–1090.
68. Kretzschmar, R.; Schäfer, T. Metal Retention and Transport on Colloidal Particles in the Environment. *Elements* **2005**, *1* (4), 205–210.
69. Cromières, L.; Moulin, V.; Fourest, B.; Guillaumont, R.; Giffaut, E. Sorption of Thorium onto Hematite Colloids. *Radiochim. Acta* **1998**, *82*, 249–255.
70. Ismailva, L. S.; Khalili, F. I.; Abu Orabi, F. M. Thorium (IV) Removal and Recovery from Aqueous Solutions Using Modified Silica Nanoparticles with Cysteine or Methionine Amino Acids. *Desalin. Water Treat.* **2020**, *196*, 161–176.
71. Wedepohl, K. H. The Composition of the Continental Crust. *Geochim. Cosmochim. Acta* **1995**, *59* (7), 1217–1232.
72. McLennan, S.; Taylor, S. Th and U in Sedimentary Rocks: Crustal Evolution and Sedimentary Recycling. *Nature* **1980**, *285*, 621–624.